A SCDAP/RELAP5 ANALYSIS OF AN AP600 3BE TRANSIENT WITH EX-VESSEL FLOODING

D. L. Knudson

April 26, 1996

Idaho National Engineering Laboratory
Idaho Falls, ID 83415

Enclosure 2

CONTENTS

1. INTRODUCTION 1

2. SCDAP/RELAP5 ANALYSIS 2

2.1 SCDAP Input 2

2.2 RELAP5 Input 3

2.3 Lower Head Input 3

2.4 Description of Transient Simulation 5

3. RESULTS 7

4. REFERENCES 8

FIGURES

1. AP600 core cross section showing the radial division used in the subject analysis 10

2. AP600 core radial power profile 11

3. AP600 core cross section showing RCC and GRC assembly locations 12

4. Cross section of an AP600 fuel assembly with a RCC assembly 13

5. Cross section of an AP600 fuel assembly with a GRC assembly 13

6. Existing AP600 RELAP5 model nodalization 14

7. AP600 core cross section showing axial nodalization (without the thimble bypass and the core cross flow junctions) 15

8. AP600 core axial power profile 16

9. Cross section of the AP600 reactor vessel lower wall and lower head 17

10. Finite element mesh representing the AP600 reactor vessel lower wall and lower head 18

11. Nusselt number ratio as a function of the angle from molten pool centerline 19

12. Azimuthal position of major AP600 vessel penetrations 19

13. MAAP containment pressure[8] used as a SCDAP/RELAP5 boundary condition 20

14. MAAP containment vapor temperature[8] used as a SCDAP/RELAP5 boundary condition 20

15. MAAP containment water level[8] used as a SCDAP/RELAP5 boundary condition 21

16. Orientation for calculation of boiling heat transfer from a hemispherical surface 21

17. Predicted heat flux to a subcooled pool from lower head heat transfer correlations as a function of position and temperature difference[6,7] 22

18. RCS and containment pressures 22

19. DVI2 break flows 23

20. DVI2 integrated break flows 23

21. Accumulator liquid volumes 24

22. CMT collapsed liquid volumes 24

23. Core collapsed liquid level relative to the bottom of the lower core plate 25

24. Calculated core collapsed liquid level compared to ROSA/AP600 experimental data[14] relative to the bottom of the lower core plate 25

25. Reactor vessel liquid mass 26

26. Maximum core surface temperature 26

27. Total hydrogen generated 27

28. ADS1 flow 27

29. ADS1 integrated flow 28

30. ADS2 flow 28

31. ADS2 integrated flow 29

32. ADS3 flow 29

33. ADS3 integrated flow 30

34. ADS4 flows 30

35. ADS4 integrated flows 31

36. Average core outlet vapor temperature 31

37. Fraction of fission products released from the fuel 32

38. Decay power distribution 32

TABLES

1. SCDAP components used to represent the AP600 core 33

2. Material masses in the active core region represented by SCDAP components 34

3. Coefficients used in a subcooled nucleate boiling correlation as a function of position on the exterior surface of the reactor vessel lower hemispherical head 34

4. Subcooled boiling correlations and CHF for nodes on the exterior surface of the COUPLE mesh 35

5. Sequence of transient events 36

6. Summary of relocation events 38

A SCDAP/RELAP5 ANALYSIS OF AN AP600 3BE TRANSIENT WITH EX-VESSEL FLOODING

1. INTRODUCTION

Accidents involving full reactor coolant system (RCS) depressurization and failure of gravity injection into the reactor vessel from the in-containment refueling water storage tank (IRWST) are the largest contributors to AP600 core damage frequency. A SCDAP/RELAP5[1] analysis of such accidents, which are identified as 3BE transients, was recently completed to evaluate lower head integrity.[2] That analysis considered accidents initiated by a double-ended off-set break in one of two direct vessel injection (DVI) lines. Three variations of the transient were considered including a case with a dry reactor vessel cavity, a case with a sustained cavity water level at the top of the reactor vessel lower hemispherical head, and a case with a sustained reactor vessel cavity water level above the break (which led to vessel reflooding).

Results from the recently completed analysis indicated that the lower head would fail by melting following the relocation of core materials with or without ex-vessel flooding. The importance of lower head integrity prompted a thorough review of those results. The review indicated a need for a revised analysis with recommended SCDAP/RELAP5 code and AP600 input model refinements to be used in the calculation of lower head response. The revised analysis is the subject of this report.

Code refinements that were recommended and incorporated into this analysis included a modification for the appropriate decay of power in the low[illegible]d debris, extension of molten pool natural convection heat transfer calculations after complete abla[illegible]lting of any frozen oxide materials on inner vessel surfaces, and adjustment of molten pool natural convection heat transfer correlations consistent with current recommendations[3]. Those refinements were incorporated into Version 8dl of the code. Version 8dl, which was the most current version and a pre-MOD 3.2 release, offered the advantage of including other code corrections and refinements that were developed since completion of the earlier analysis. (It should be noted that recommendations were also made for the addition of dead load and buoyancy [as a result of the ex-vessel flooding] forces in lower head integrity calculations and solution algorithm modifications to improve time step performance, particularly during the low pressure core oxidation phase. However, a dead load/buoyancy evaluation indicated that SCDAP/RELAP5 refinement was not justified because the specified forces are insignificant compared to the temperature-dependent ultimate strength of the vessel wall.[4] Work was also initiated on solution algorithm modifications to improve time step performance, but those modifications were not completed in time to be used.)

AP600 input model refinements that were recommended and incorporated into this analysis included reactor kinetics input for a best-estimate calculation of decay heat[5], extension of the lower head finite element mesh to avoid any potential for thermal isolation (at the top of the debris bed) imposed by the current version of the code if the mesh is fil!ed, a 3.3 K (6 °F) increase in steady state loop operating temperatures consistent with current design specifications, adoption of subcooled boiling correlations for ex-vessel heat transfer (based on experimental data[6,7]), use of an ex-vessel flooding history from a previous MAAP calculation[8], and addition of input to model stainless steel slumping if internal vessel structures are predicted to melt. Those refinements were incorporated into Version 3.0 of the simplified AP600 model.[9] Version 3.0, which was the most current version, offered the advantage of including other AP600 design changes that have been announced since completion of the earlier analysis.

Like the earlier analysis, lower head failure is assumed if heat loads exceed the CHF or creep rupture is calculated. In addition, a double-ended off-set break in one of two DVI lines was assumed to be the transient initiator. In this revised analysis, however, the reactor vessel cavity water level was assumed to increase as a function of time until reaching a sustained level above the break (consistent with the previous MAAP calculation[8]). Although ex-vessel flooding resulted in a sustained cavity water level above the break, vessel reflooding was not considered. That modeling decision was made to allow direct comparison with a current MAAP calculation at a future date.[10]

The SCDAP/RELAP5 model and details associated with the transient simulation are described in Section 2, calculated results through the time of core relocation are outlined in Section 3, and references are listed in Section 4. Calculations to evaluate lower head response to the core relocation are in progress. A revision of this report is anticipated after the lower head calculations and a comparison with the current MAAP calculation are complete.

2. SCDAP/RELAP5 ANALYSIS

SCDAP/RELAP5 is an integrated computer code package designed for nuclear reactor accident analysis. Modules for simulation of severe core damage, thermal-hydraulics, and heat transfer are included. The user may develop input for those modules needed to simulate the problem of interest. In this analysis, an appropriate model required SCDAP input to simulate AP600 core components (including fuel rods, control rods, gray rods, instrumentation thimbles, empty guide thimbles, grid spacers, intermediate flow mixing [IFM] spacers, and the stainless steel reflector); RELAP5 input to represent thermal-hydraulics in the core, throughout the remainder of RCS, and in selected portions of the secondary systems; and finite element input to represent the lower head during any thermal attack associated with relocated core materials. Corresponding input descriptions for those modules are provided in Sections 2.1, 2.2, and 2.3, respectively. Details specifically associated with the transient simulation are described in Section 2.4.

2.1. SCDAP Input

The radial division of the AP600 core, shown in Figure 1, was the basis for all SCDAP input developed for this analysis. Specifically, the division was established to reflect the AP600 radial power profile (shown in Figure 2) and define parallel paths for axial flow through the core. (It should be noted that the assembly relative power was normalized for an unrodded core at hot full power with equilibrium xenon near the beginning of life, which appeared to be the best data available.) Once the radial nodalization was established, the number of fuel assemblies, rod cluster control (RCC) assemblies, and gray rod cluster (GRC) assemblies within each radial division/flow channel could be determined as indicated in Figure 3. That information and the RCC and GRC assembly cross sections shown in Figures 4 and 5, respectively, were then used to develop input for each of the components summarized in Table 1.

The stainless steel reflector, which is not illustrated, was modeled as two components connected to the outer radial division/flow channel as indicated in Table 1. That approach was used because the reflector consists of a relatively thin flat section and a thicker section that was fabricated to fit the core barrel arc. The use of two components allowed a more accurate representation of the thermal mass and resistance of each section, which should result in a better approximation of reflector heating. An appropriate area was provided within each reflector component to represent embedded flow holes.

There are four IFM spacers, two Inconel grid spacers, and seven Zircaloy grid spacers in the AP600 core. Input was developed to represent all four IFM spacers and the seven Zircaloy grid spacers in the SCDAP model. The two Inconel spacers were not explicitly simulated because they lie outside (above and below) the active core region that can be modeled with the current version of SCDAP. However, loss coefficients were appropriately included to provide hydraulic simulation. A summary of all material masses specified through SCDAP input is provided in Table 2.

2.2. RELAP5 Input

Input used to simulate AP600 thermal-hydraulics was based on an existing RELAP5 model shown in Figure 6. The model includes the reactor vessel; both primary coolant loops; all four primary coolant pumps; the pressurizer; passive safety systems (including accumulators, an automatic depressurization system [ADS], core makeup tanks [CMTs], the IRWST, and a passive residual heat removal [PRHR] system); selected portions of the secondary systems as necessary to complete the subject analysis, and associated heat structures. Additional details regarding the RELAP5 model are available in existing documentation.[9] It should be noted that PRHR piping downstream of the ADS4 tee (numbered 832, 833, 834, 835, 836, 838, and 839) and IRWST drain piping (numbered 811 through 817 and 821 through 827) were deleted because those systems were assumed to fail in this analysis.

In order to simulate core damage, existing RELAP5 flow paths and heat structures representing the active core region (numbered 114, 115, 116, 121, and 122) had to be replaced with the SCDAP components described in Section 2.1. The region affected by that substitution is shown in Figure 7. Five radial divisions defining axial flow paths through the core are shown, consistent with Figures 1 and 3. The axial flow paths, with the axial power profile shown in Figure 8, were cross flow connected at each elevation. As indicated, cavity bypass and embedded reflector flow holes were connected to the outer core flow channel.

2.3. Lower Head Input

A detailed representation of the reactor vessel lower hemispherical head was needed to evaluate lower head response following the relocation of core materials. In addition, a representation of some portion of the reactor vessel cylindrical wall had to be considered. A portion of the cylindrical wall had to be included because the current version of the code will set heat transfer from the top of the debris bed to zero if the total volume considered is too small to contain all relocated materials. In this case, a relatively large portion of the cylindrical wall was included along with the lower head (as indicated in Figure 9) so that the corresponding volume cannot possibly fill. The portion of wall considered should also be adequate for simulation of any axial conduction effects.

The specified lower head and cylindrical wall region was represented by the finite element mesh shown in Figure 10, which replaced corresponding RELAP5 heat structures. The axisymmetric mesh included a total of 572 nodes with 525 elements. Three elements were used to represent the combined thickness of the carbon steel wall and the stainless steel liner. Those wall elements, which were modeled as a homogeneous slab of carbon steel since the liner is relatively thin, are defined by Nodes 1 through 88 as shown in the figure. A layer of zero-width gap elements was aligned with the inner surface of the liner (Nodes 67 through 110) to provide a way to represent the contact resistance between the debris and the vessel. A constant coefficient of 500 W/m^2-K was used to represent that resistance. The remaining ele-

ments were initially filled with primary coolant, which can boil off and/or be displaced during relocation of molten core materials.

After molten materials collect in the lower head, SCDAP/RELAP5 calculates natural convection heat transfer at interfaces between the molten pool and adjacent solid materials. That heat transfer is based on average coefficients from steady state correlations. Specifically, the mean heat transfer coefficient to the upper crust covering the molten pool was developed by Steinberner and Reineke[11] and is given by

$$h_u = \frac{k}{R} 0.345 Ra^{0.233} \tag{1}$$

while the mean downward heat transfer coefficient applicable to all other surfaces was developed by Mayinger[12] and is given by

$$h_d = \frac{k}{R} 0.54 Ra^{0.18} \tag{2}$$

where

- k = thermal conductivity of the melt in the boundary layer adjacent to the interface,
- R = effective radius of the molten region (based on the volume of all molten elements in an assumed hemispherical geometry), and
- Ra = Rayleigh number associated with the molten pool.

The Rayleigh number is defined as

$$Ra = \frac{g\beta Q R^5}{\alpha \nu k} \tag{3}$$

where

- g = gravitational constant,
- β = coefficient of volumetric expansion,
- Q = volumetric heat generation rate,
- α = thermal diffusivity and
- ν = kinematic viscosity of the molten materials.

Experiments conducted by Jahn and Reineke indicate that the local downward heat transfer coefficient is a function of the angular position from the centerline of the molten pool.[13] Specifically, the ratio of the local Nusselt number to the mean Nusselt number (Nu_l/Nu_m) varies from ~0.15 at $\theta = 0^o$ to ~1.5 at $\theta = 90^o$ in a hemispherical geometry. That result is approximated in SCDAP/RELAP5 as shown in Figure 11. Accordingly, calculation of natural convection heat transfer from the lower head molten pool to the vessel wall involves identification of molten finite elements adjacent to elements containing solid materials, use of Equation (1) or (2) to determine the appropriate heat transfer coefficient, and application of the analytical representation of Figure 11 to modify the downward coefficients as a function of angular position.

Heat transfer from the molten pool through the vessel wall was then rejected into containment through the exterior surface of the lower head (Nodes 1 through 22 shown in Figure 10). A discussion of that boundary condition is provided in the following section since it is transient specific.

2.4. Description of Transient Simulation

The transient-initiating break was assumed to occur at time zero in the DVI2 line, which is shown relative to other major AP600 vessel penetrations in Figure 12. (Note that the position of the DVI lines relative to hot leg one [HL1] is of interest because the pressurizer is connected to HL1 and because the pressurizer represents the only potentially significant asymmetry of interest. As indicated, however, the DVI lines are positioned symmetrically with respect to HL1 and the pressurizer. Consequently, the break could have been modeled in either DVI line without a significant impact on the results.) The break was opened between the (0.102 m) DVI2 flow venturi and the flow restrictors downstream of the accumulator, CMT2, and the IRWST. Since the DVI2 line has an inside diameter of 0.173 m, each side of the double-ended off-set break was assigned a flow area of 0.0235 m^2. However, break flow was actually controlled by the DVI2 venturi and the other flow restrictors. (A flow coefficient of 0.8 was applied to both DVI venturis, which is consistent with the current practice in ongoing RELAP5 analyses of AP600.) All break flow was appropriately directed into containment.

AP600 containment was represented by an adiabatic volume in the existing RELAP5 input model. However, that approach is not adequate for simulation of containment response in long term transients because condensation is not represented. Although existing RELAP5 input could have been modified to account for condensation, a decision was made to use the containment pressure from a MAAP calculation[8] as a time-dependent boundary condition for break and ADS flows. That pressure is shown in Figure 13.

Consistent with the definition of 3BE transients, gravity injection from the IRWST was assumed to fail. In addition, the PRHR system and one train of the ADS (one of two ADS1 valves, one of two ADS2 valves, one of two ADS3 valves, and two of four ADS4 valves) were assumed to fail. Both accumulators and CMTs were assumed to be available. However, the inventories of one accumulator and one CMT were lost to containment through the passive safety system end of the DVI2 line break.

Initially, heat was transferred from the exterior surface of the lower head (Nodes 1 through 22 shown in Figure 10) to a dry containment environment using a constant coefficient of 75 W/m^2-K and a MAAP containment air temperature[8]. The coefficient was assumed to be reasonable for simulating convective heat losses to containment. The MAAP temperature, shown in Figure 14, was used as the sink temperature in lieu of modifying RELAP5 containment input (as previously discussed).

The dry containment environment was altered relatively early in the subject transient because a portion of RCS, accumulator, and CMT inventories collect in the reactor vessel cavity after break initiation. In addition, it was assumed that operators initiate cavity flooding (using IRWST drain lines) at the time core outlet vapor temperatures reach 1366 K. The MAAP prediction of the resulting water level[8], which is shown in Figure 15, was used in this analysis because the required containment input was not included in the existing RELAP5 model. Accordingly, heat transfer from the exterior surface of the lower head shifted from an air convective mode to a water convective/boiling mode as each surface node was submerged as discussed below.

A set of subcooled nucleate boiling correlations[6] were developed for calculation of heat flux (in W/m^2) from a hemispherical surface in the form

$$q = a\Delta T + b\Delta T^2 + c\Delta T^3 \quad (4)$$

where

a, b, and c = position-dependent coefficients from Table 3 for the orientation shown in Figure 16 and

ΔT = the difference between the wall surface temperature and the pool saturation temperature (in K).

Nucleate boiling curves derived from Equation (4) are valid from a ΔT of ~4 K to the ΔT associated with the critical heat flux (CHF) for subcooled boiling (in MW/m^2) given by[7]

$$q_{chf} = 0.4\,(1 + 0.036\,\Delta T_{sub})\,(1 + 0.021\theta - (0.007\theta)^2) \quad (5)$$

where

ΔT_{sub} = 10 K (assumed to be a constant in this analysis) and

θ = the surface contact angle in degrees for the orientation shown in Figure 16.

Experimental data embodied in Equations (4) and (5) were then applied to each lower head surface node (numbered 1 through 22 in Figure 10) to simulate natural convection, nucleate boiling, and transition boiling regimes as follows.

- Equation (4) was used to calculate a position-dependent heat flux for ΔT = 4 K. Linear interpolation between zero and the resulting flux (at ΔT = 4 K) was performed to estimate the flux for any ΔT from 0 to 4 K, which should adequately simulate natural convection to a subcooled pool.

- Equations (4) and (5) were solved simultaneously to determine the position-dependent ΔT associated with the CHF. (Resulting CHF values are summarized for all surface nodes in Table 4.) Equation (4) was then applied to determine the subcooled nucleate boiling flux for any ΔT between 4 K and the ΔT at the CHF.

- The transition boiling heat flux was linearly extrapolated from the position-dependent CHF to the minimum flux that could occur assuming a heat transfer coefficient of 375 W/m^2-K. The extrapolation was performed for any ΔT greater than the ΔT at the CHF based on an estimate of the slope associated with transition regime experimental data.

Application of the data is depicted graphically in Figure 17 for several positions on the exterior surface of the lower head. It should be noted that experimental data for the film boiling regime were not provided; although the lack of that data is not expected to be important because lower head failure will be assumed if heat fluxes from core materials in the lower head are high enough to drive the exterior surface beyond the CHF. (The potential effects associated with creep damage are also considered in evaluation of lower head integrity.) As previously indicated, however, calculation of lower head response (based on the foregoing) is in progress. A revision of this report is anticipated when the lower head calculations and a comparison with the current MAAP calculation are complete.

3. RESULTS

A double-ended off-set-break in the DVI2 line was opened (between the DVI2 flow venturi and the flow restrictors downstream of the accumulator, CMT2, and the IRWST) to initiate the transient at time zero. A sequence of key events that developed thereafter is summarized in Table 5, which may be helpful in conjunction with the following discussion.

The break flows led to a rapid RCS pressure reduction (from an initial pressure of 15.51 MPa) as indicated in Figure 18. That pressure reduction triggered a reactor scram at 10.89 s. Continued flow through the breaks (see Figures 19 and 20) resulted in actuation of both CMTs by 12.86 s. The accumulator and CMT connected to the DVI2 line drained directly into containment through the passive safety system side of the break and, consequently, emptied relatively early as indicated in Figures 21 and 22. Flows from the accumulator and CMT connected to the intact DVI line (DVI1) were directed into the vessel, but they did not prevent an early uncovery of the top of the active fuel as shown in Figure 23.[a] However, a relatively cool two-phase mixture in the upper half of the core was maintained by inventories from that accumulator and CMT, which was sufficient to delay core heatup as shown in Figure 26. When the accumulator and CMT connected to the DVI1 line emptied, the two-phase mixture in the upper half of the core was gradually replaced by superheated vapor as core heatup progressed. Oxidation followed (see Figure 27) as the core temperatures approached the appropriate reaction temperature range. The energy associated with the exothermic oxidation reaction led to rapid core heating and, ultimately, the first fuel melting at 6595 s.

The ADS was triggered by decreasing CMT levels. Specifically, ADS1 was actuated at 176.2 s because the CMT2 level dropped to 67.5%. The resulting flow and integrated flow from the ADS1 valve are plotted in Figures 28 and 29, respectively. (The actuation timing for remaining ADS valves is given in Table 5. Corresponding flow information is provided in Figures 30 through 35 for reference.) ADS actuation is an important phase of AP600 accident mitigation since it is normally needed to reduce RCS pressures so that gravity injection of water from the IRWST can reflood the core and arrest any heatup. In this transient, however, IRWST gravity injection was assumed to fail. Given that assumption, the IRWST can be used to flood the reactor vessel cavity in an alternate strategy to try to preserve vessel integrity.

A core outlet vapor temperature of 1366 K will be used as the signal for operator initiation of AP600 reactor vessel cavity flooding through IRWST drain lines. In this analysis, a temperature of 1366 K (based on an average of temperatures at the top of Flow Channels 113 and 114) was reached by 5666 s as indicated in Figure 36. As previously discussed, however, cavity flooding was not explicitly calculated in this analysis. Instead, the flooding history from a MAAP calculation[8] shown in Figure 15 was used as a boundary condition. From that figure, it appears that MAAP reflooding did not begin until ~6450 s. (The water level of ~2.4 m shown prior to the reflood is presumably consistent with the portion of RCS, accumulator, and CMT inventories that would collect in the cavity as a result of the DVI line break.) The discrepancy in the initiation of cavity flooding is not particularly critical in this analysis because flooding is well ahead of any core relocation into the lower head. As previously discussed, heat transfer from the exterior surface of the reactor vessel lower head (and lower wall) shifted from a vapor convection mode to a convection/subcooled nucleate boiling mode as the cavity flooded.

---

a. It is important to note that the SCDAP/RELAP5 core liquid level for first 1000 s compares closely with the level measured during a DVI line break experiment conducted in the ROSA/AP600 test facility[14] as indicated in Figure 24. After ~1000 s, the ROSA/AP600 level began to increase (and the ROSA/AP600 level began to deviate from the calculated level) as a result of IRWST injection, which was assumed to fail in this analysis. The calculated reactor vessel liquid mass is provided in Figure 25 as an additional reference.

Core uncovery was completed by 10 350 s with core melt spreading radially and axially to the reflector boundary shortly thereafter (by 10 780 s). The heat flux from the in-core molten pool to the reflector was much larger than the heat that could be removed by steam in the core barrel/reflector cavity. Consequently, the reflector was predicted to melt relatively quickly (by 10 970 s). An assumption of local reflector melting is embodied in the current version of SCDAP/RELAP5. That assumption appears to be reasonable given the asymmetries that would be expected in the core region due to the location of the break and the potential temperature variations that could develop in the vicinity of major vessel penetrations. Given that assumption, the code allowed a side-way relocation of all molten materials, at or above the location of reflector failure, into the lower head without addition of reflector stainless steel. The timing, composition, and temperature of the associated relocation (and all other predicted relocations) are summarized in Table 6.

Four subsequent side-way relocations followed as molten materials spread to intact reflector boundaries at progressively lower core levels (see Tables 5 and 6). A final relocation through the bottom of the core followed. Specifically, molten materials reached the bottom of the fueled region by 12 840 s. At that time, the code allowed relocation into the lower head based on the assumption that the melt could flow through holes in the lower core support plate and/or melt through the reflector in order to complete the relocation. In total, ~64 000 kg of molten fuel, or ~85% of the AP600 active core, was relocated to the lower head during the transient. Other lower head debris constituents are identified in Tables 5 and 6. Calculations are in progress to evaluate lower head response to the relocated materials. A revision of this report is anticipated when those calculations are complete.

Between 60 and 70% of the volatile fission products were released from the fuel during the core degradation process (see Figure 37). The corresponding effect of fission product release on core decay power is illustrated in Figure 38. Specifically, the total decay power was reduced by ~14% (calculated at the time of the first relocation) as a result of the fission product release that began at ~4500 s. Subsequent reductions in the core power correspond with relocations into the lower head that were discussed above. It should be noted that the single increase in (total and core) power shown in Figure 38 at 10 000 s is consistent with the American Nuclear Society Standard for the calculation of decay heat, which was appropriately considered in development of the best-estimate reactor kinetics input used in this analysis[5].

4. REFERENCES

1. C. M. Allison et al., *SCDAP/RELAP5/MOD3.1 Code Manuals, Volumes 1-5*, NUREG/CR-6150, INEL-95/0609, (formerly EGG-2720), December 1995.

2. D. L. Knudson (INEL) letter to Y. Chen (NRC), "Transmittal of Revision 1 of Task 14 Letter Report Under JCN L2230", DLK-12-95, July 7, 1995.

3. C. M. Allison et al., *Design Report on SCDAP/RELAP5 Model Improvements - Debris Bed and Molten Pool Behavior*, INEL-94/0174, November 1994.

4. S. A. Chavez (INEL) letter to Y. Chen (NRC), "Corrections Made per Telephone Conversation of July 31, 1995", SAC-8-95, October 30, 1995.

5. J. L. Judd (INEL) letter to W. Jensen (NRC), "AP600 Best-Estimate Decay Heat Input for RELAP5 based on ORIGEN2 Calculations (L2419-T10)", JLJ-09-95, October 19, 1995.

6. W. Cheung (Pennsylvania State University) fax to J. Rempe (INEL), October 25, 1994.

7. W. Cheung (Pennsylvania State University) fax to E. Coryell (INEL), February 16, 1995.

8. R. Palla (NRC) fax to D. Knudson (INEL), transmitting a summary of a MAAP calculation entitled "Description of DVI Line Break Cases", February 6, 1995.

9. G. E. Wilson (INEL) letter to T. Lee (NRC), "Benchmark of Updated AP600 Simplified Input Deck, J6008", GEW-61-95, October 27, 1995.

10. R. Palla (NRC) fax to D. Knudson (INEL), transmitting a summary of a MAAP calculation entitled "Description of DVI Line Break Cases", April 8, 1996.

11. U. Steinberner and H. H. Reineke, "Turbulent Buoyancy Convection Heat Transfer with Internal Heat Sources", *Proceedings of the 6th International Heat Transfer Conference*, August 1978.

12. F. Mayinger et al., *Examination of Thermal-Hydraulic Processes and Heat Transfer in a Core Melt*, BMFT RS 48/1, Institute for Verfahrenstechnik der T. U. Hanover, 1976.

13. M. Jahn and H. H. Reineke, "Free Convection Heat Transfer with Internal Heat Source, Calculations and Measurements", *Proceedings of the International Meeting on Thermal Nuclear Reactor Safety*, NUREG/CR-0027, February 1983.

14. R. Shaw, T. Yonomoto, and Y. Kukita, *Quick Look Report for ROSA/AP600 Experiment AP-DV-01*, JAERI-memo 07-189, September 1995.

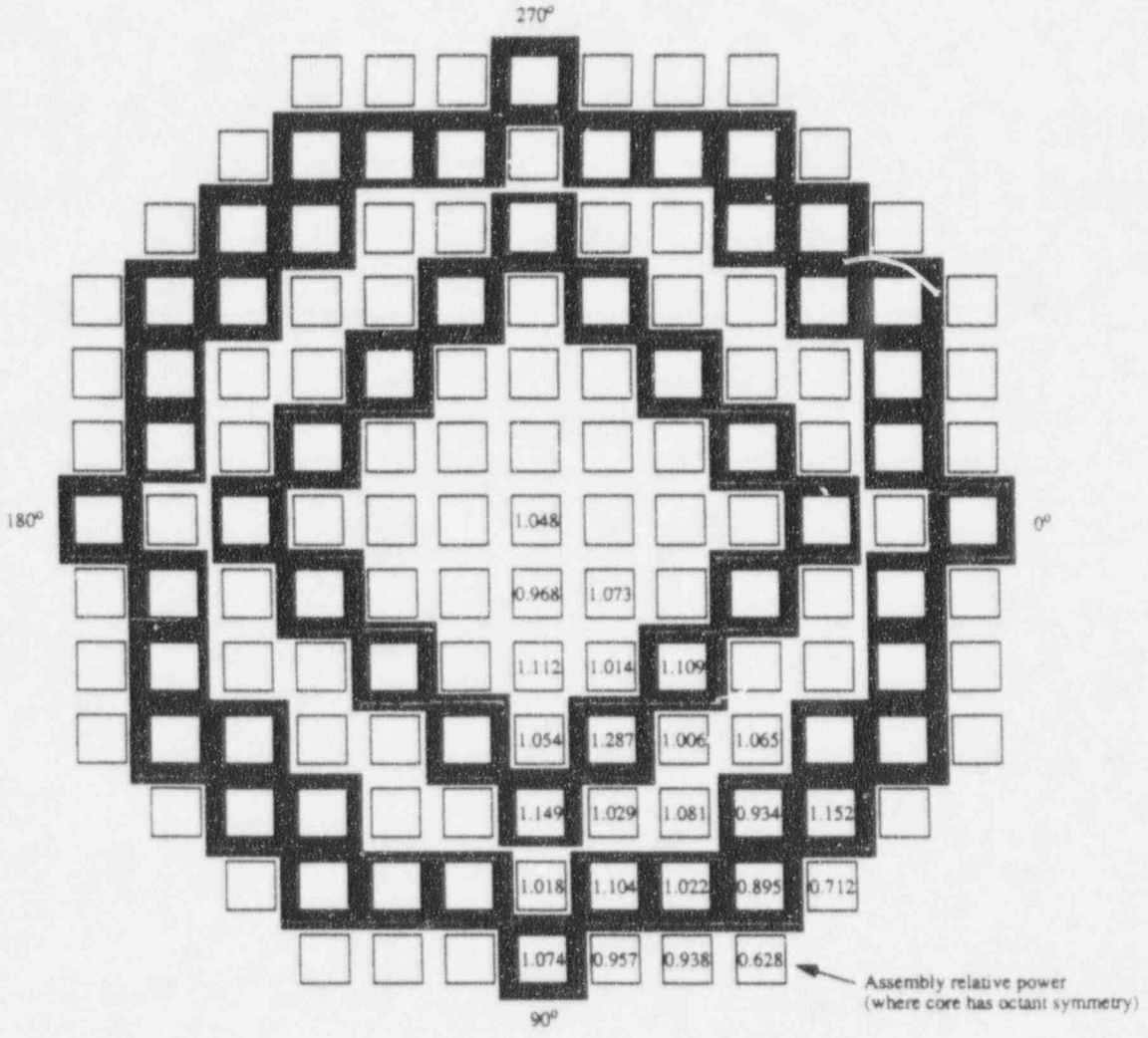

Radial Division (numbered from center to periphery)	Number of Fuel Assemblies	Relative Power	Normalized Relative Power
1	25	1.040	1.040
2	16	1.208	1.209
3	32	1.039	1.039
4	40	1.014	1.013
5	32	0.809	0.809

Figure 1. AP600 core cross section showing the radial division used in the subject analysis.

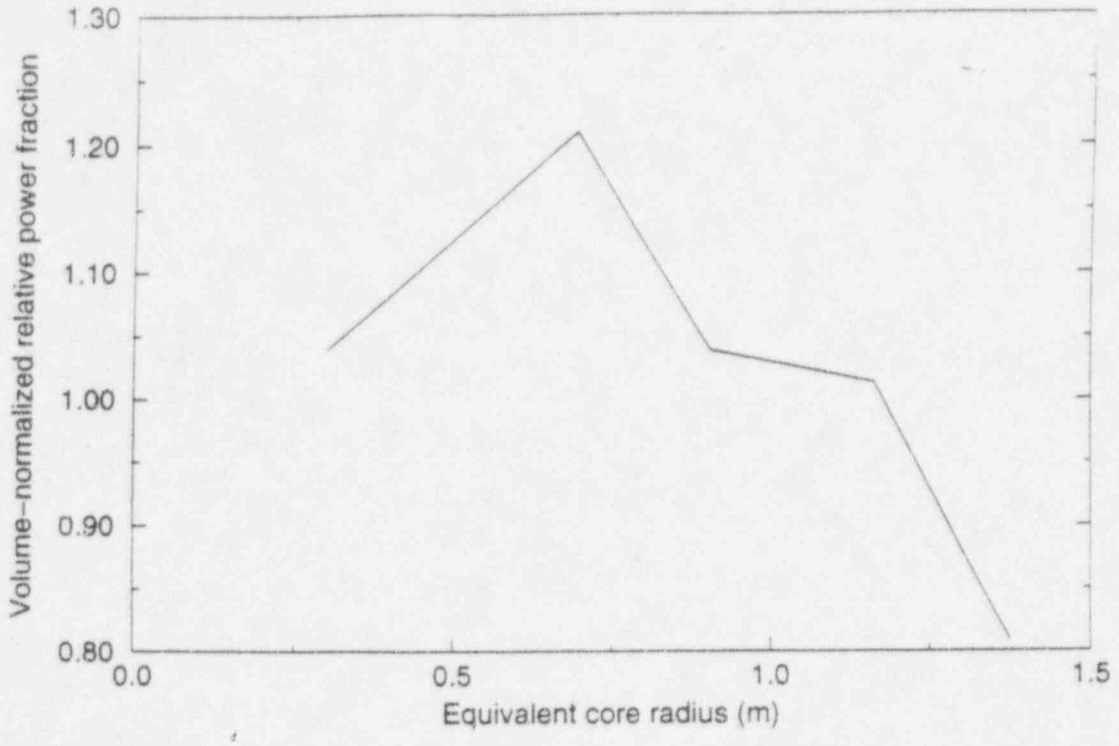

Figure 2. AP600 core radial power profile.

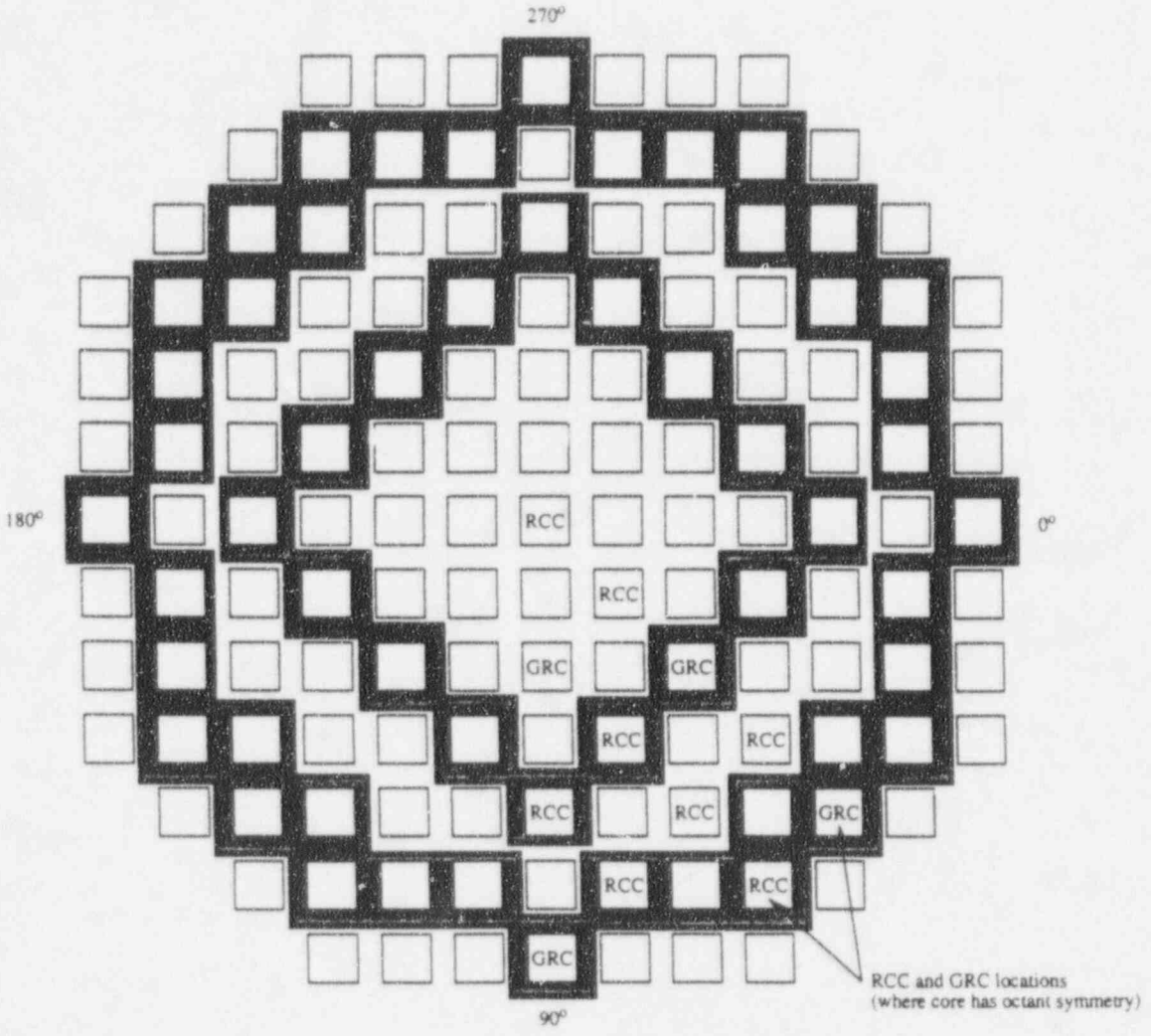

Radial Division (numbered from center to periphery)	Number of Fuel Assemblies	Number of RCCs	Number of GRCs
1	25	5	4
2	16	12	4
3	32	12	0
4	40	16	8
5	32	0	0

Figure 3. AP600 core cross section showing RCC and GRC assembly locations.

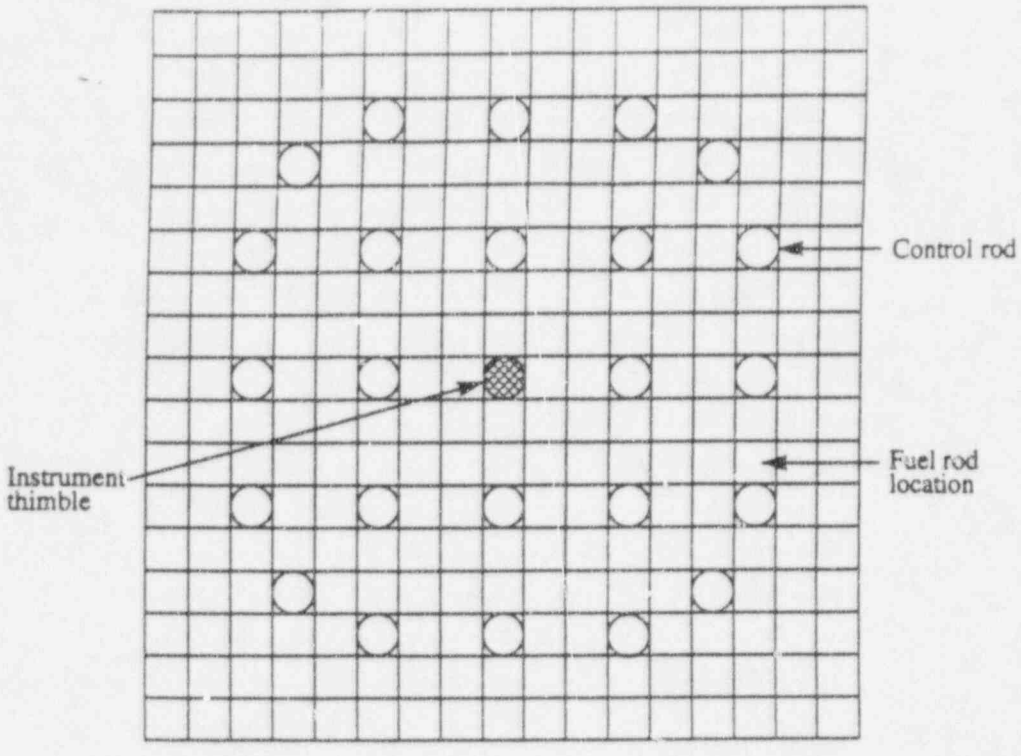

Figure 4. Cross section of an AP600 fuel assembly with a RCC assembly.

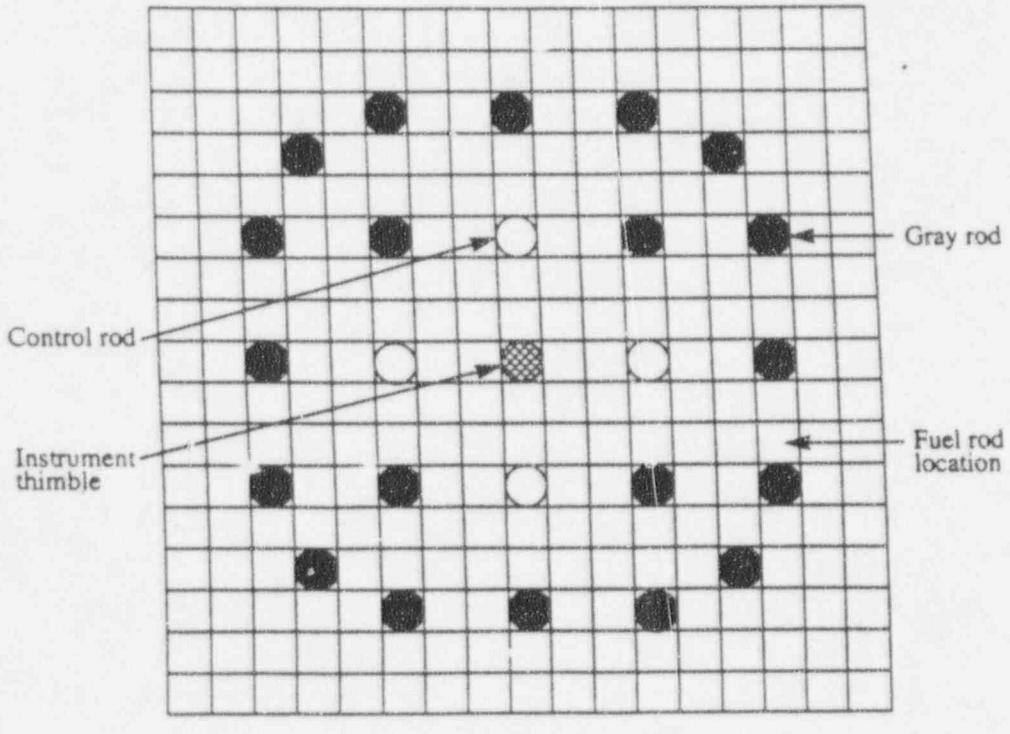

Figure 5. Cross section of an AP600 fuel assembly with a GRC assembly.

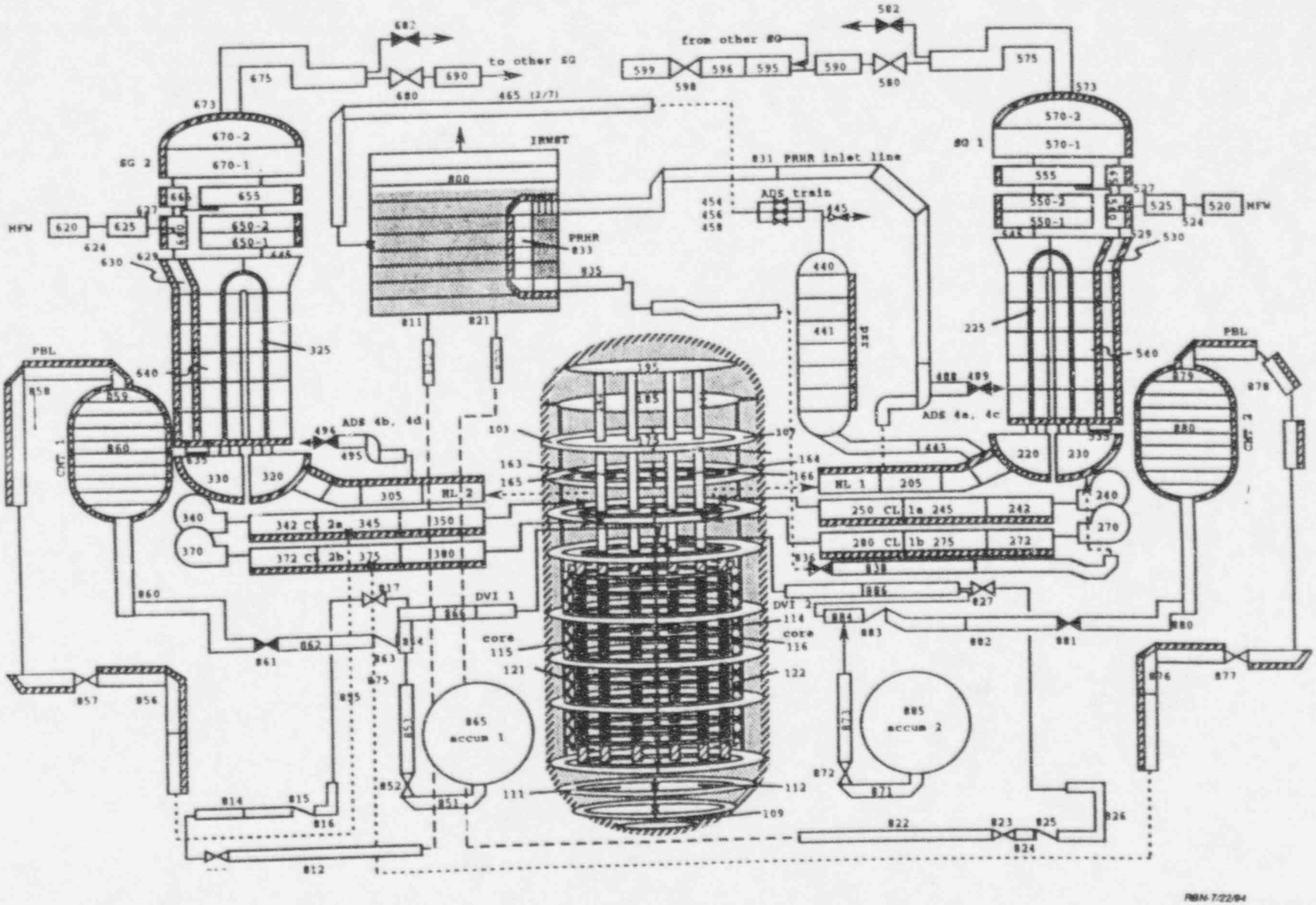

Figure 6. Existing AP600 RELAP5 model nodalization.

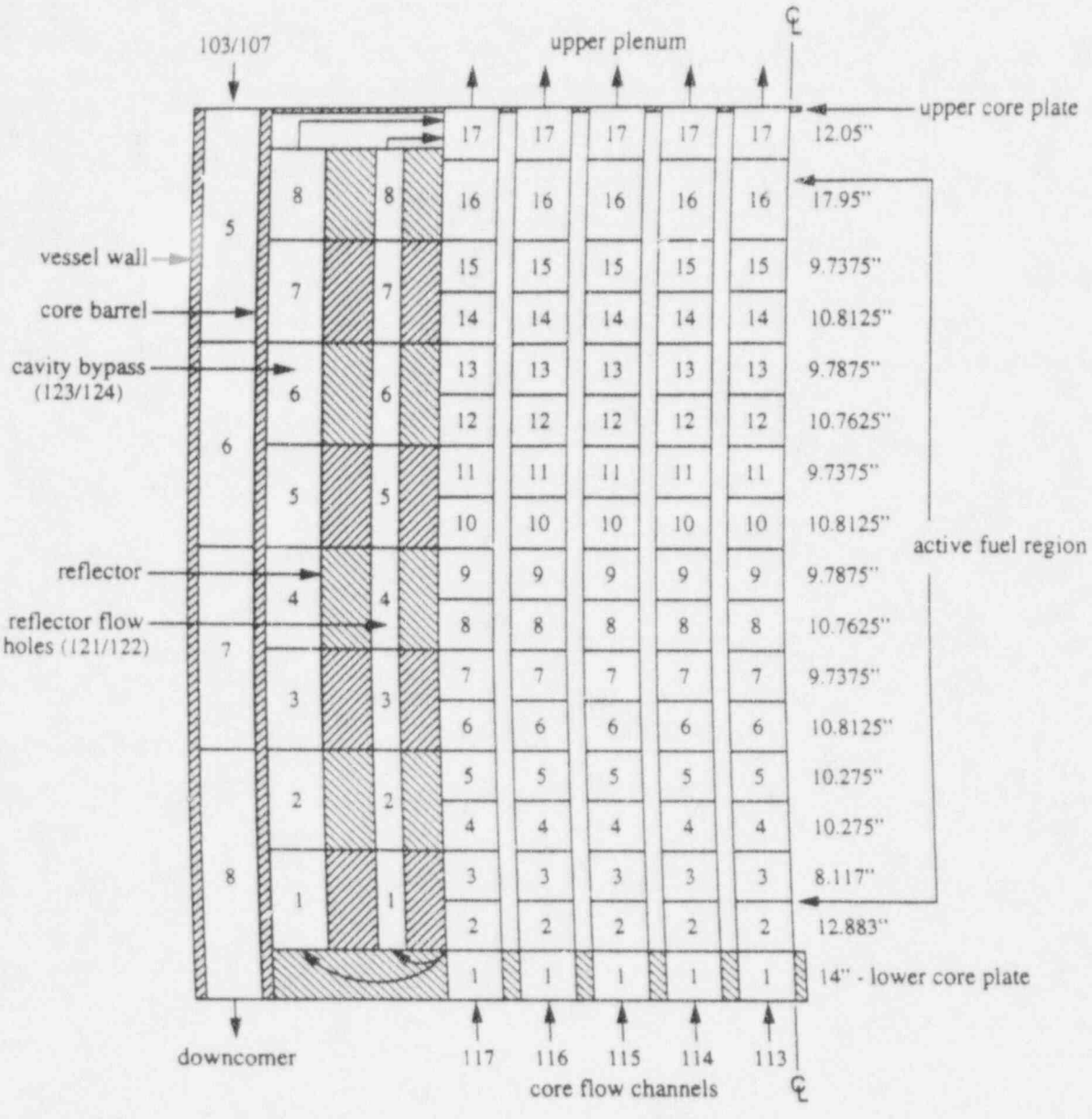

Figure 7. AP600 core cross section showing axial nodalization (without the thimble bypass and the core cross flow junctions).

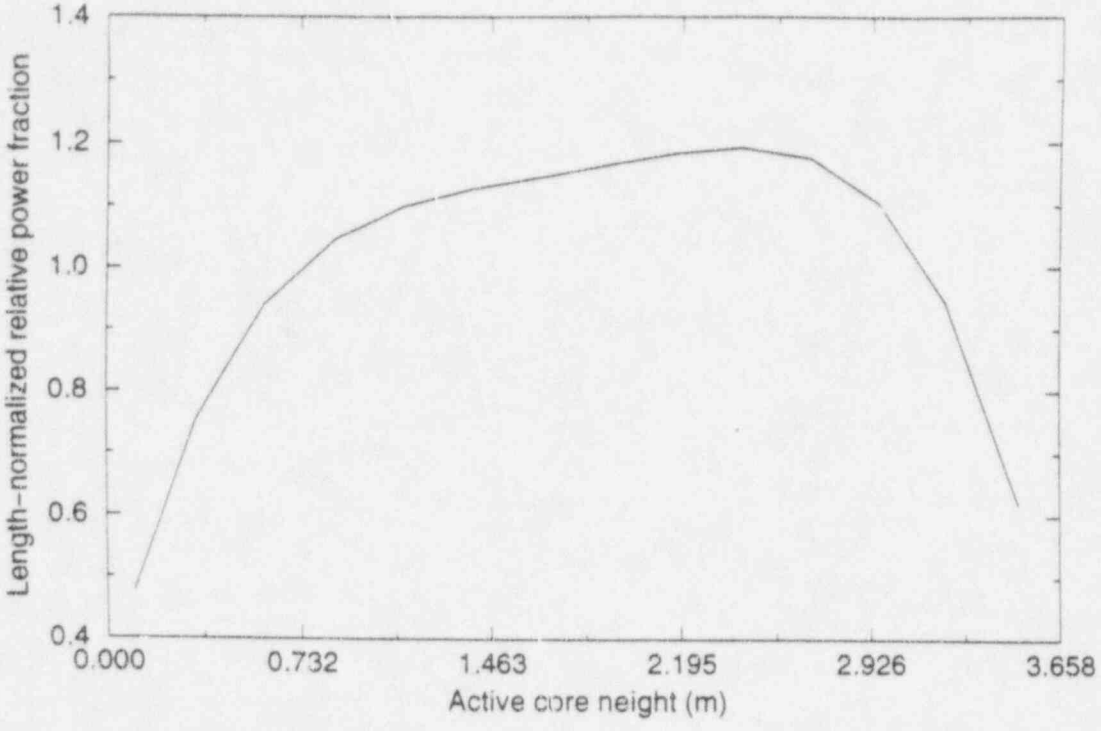

Figure 8. AP600 core axial power profile.

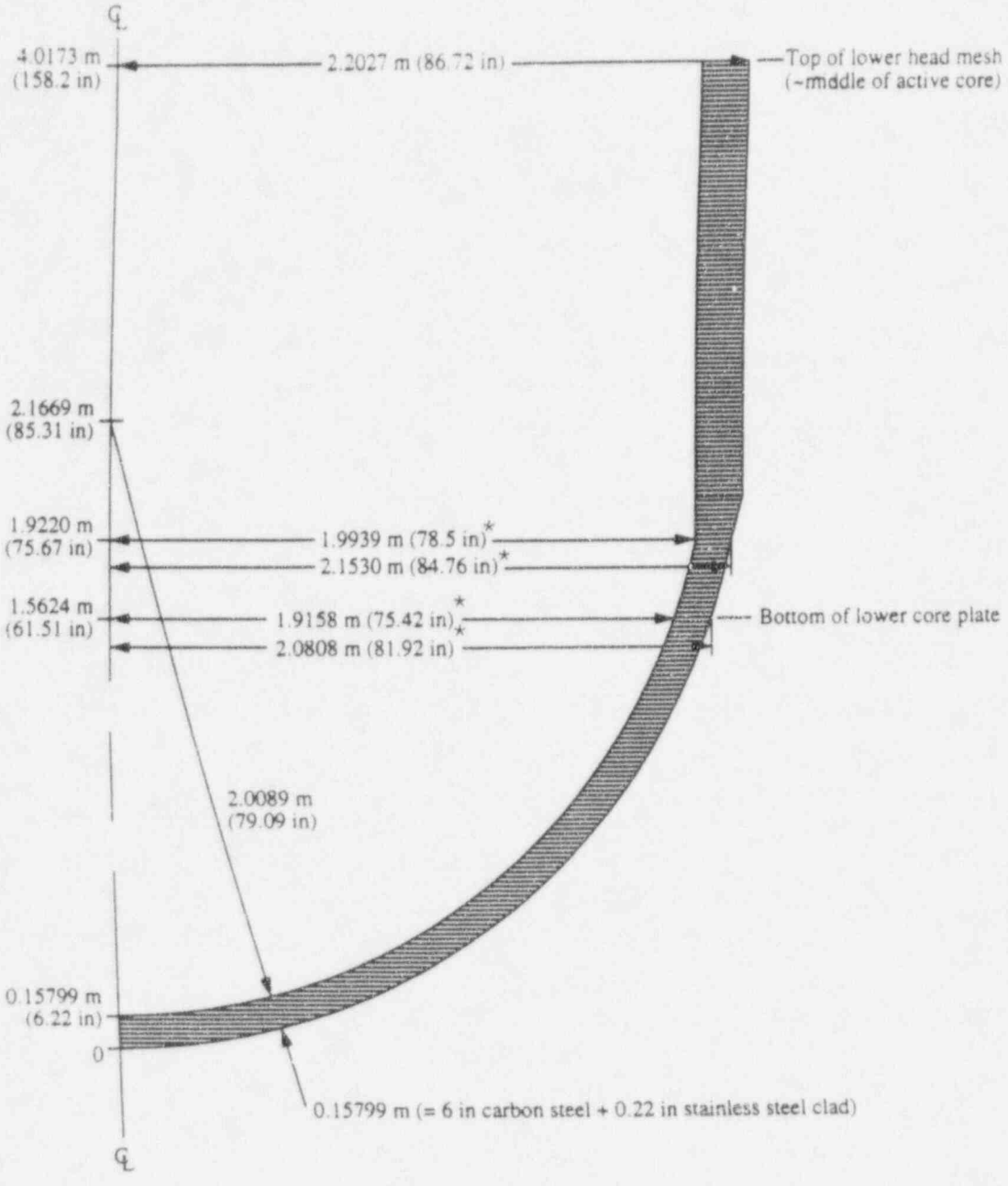

Figure 9. Cross section of the AP600 reactor vessel lower wall and lower head.

* indicates that the number was derived using engineering judgement

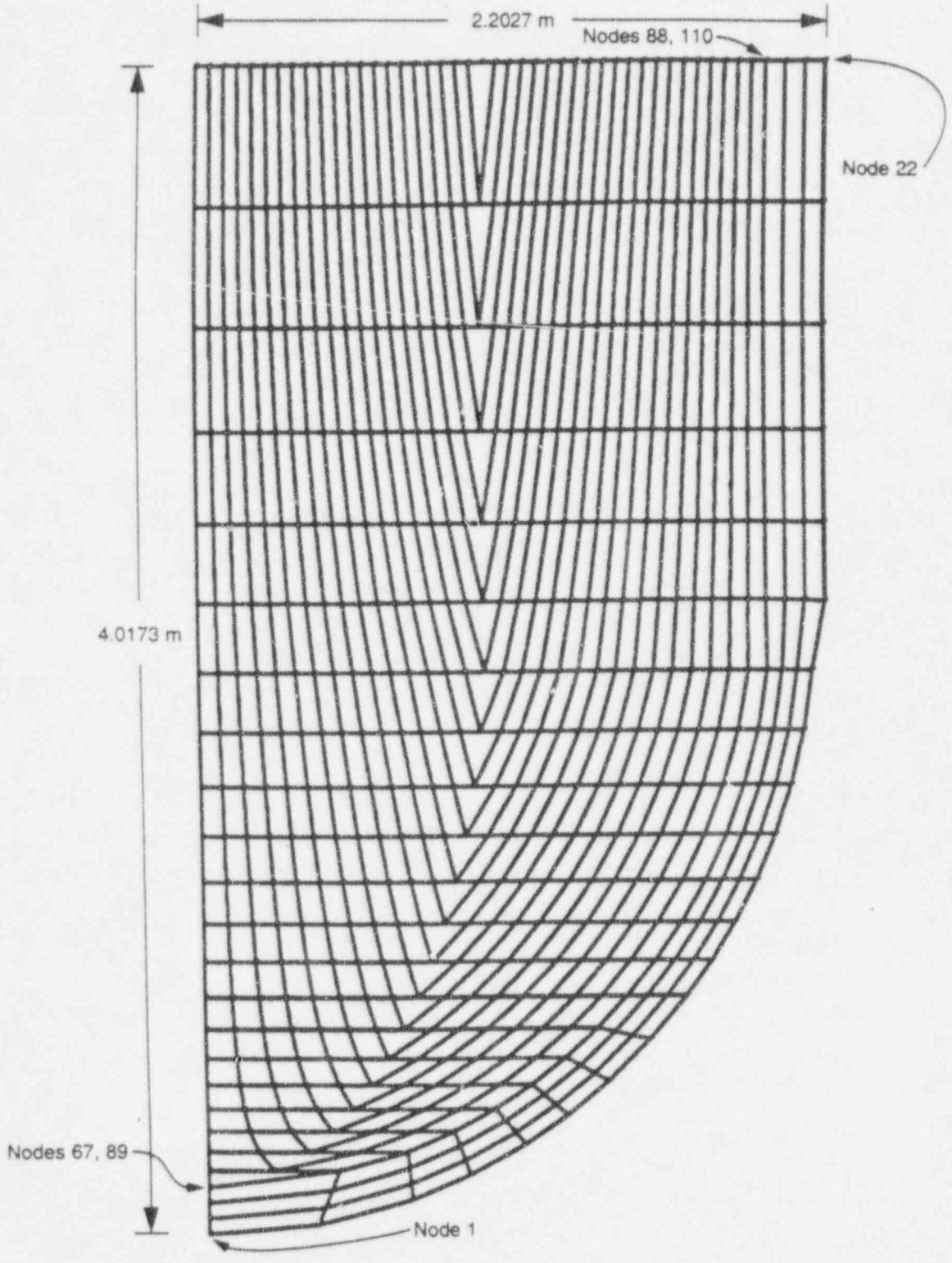

Figure 10. Finite element mesh representing the AP600 reactor vessel lower and lower head.

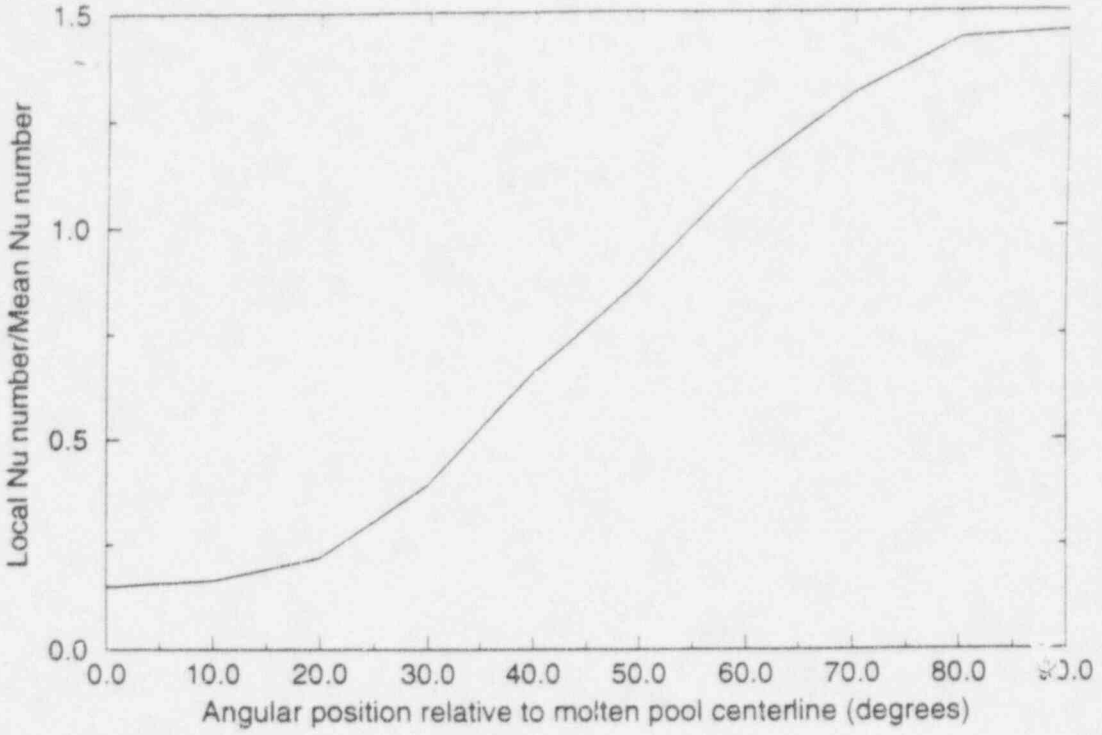

Figure 11. Nusselt number ratio as a function of the angle from molten pool centerline.

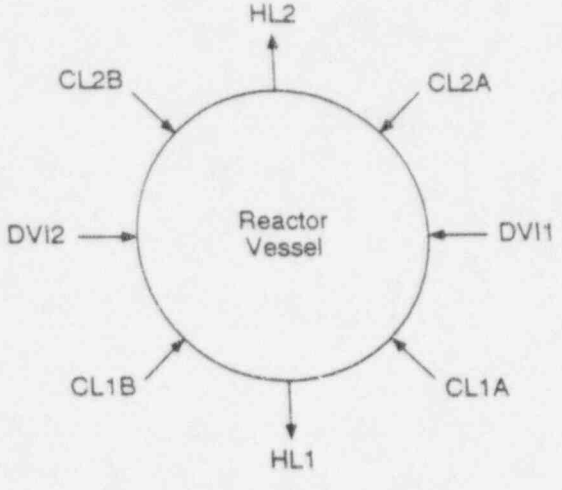

Figure 12. Azimuthal position of major AP600 vessel penetrations.

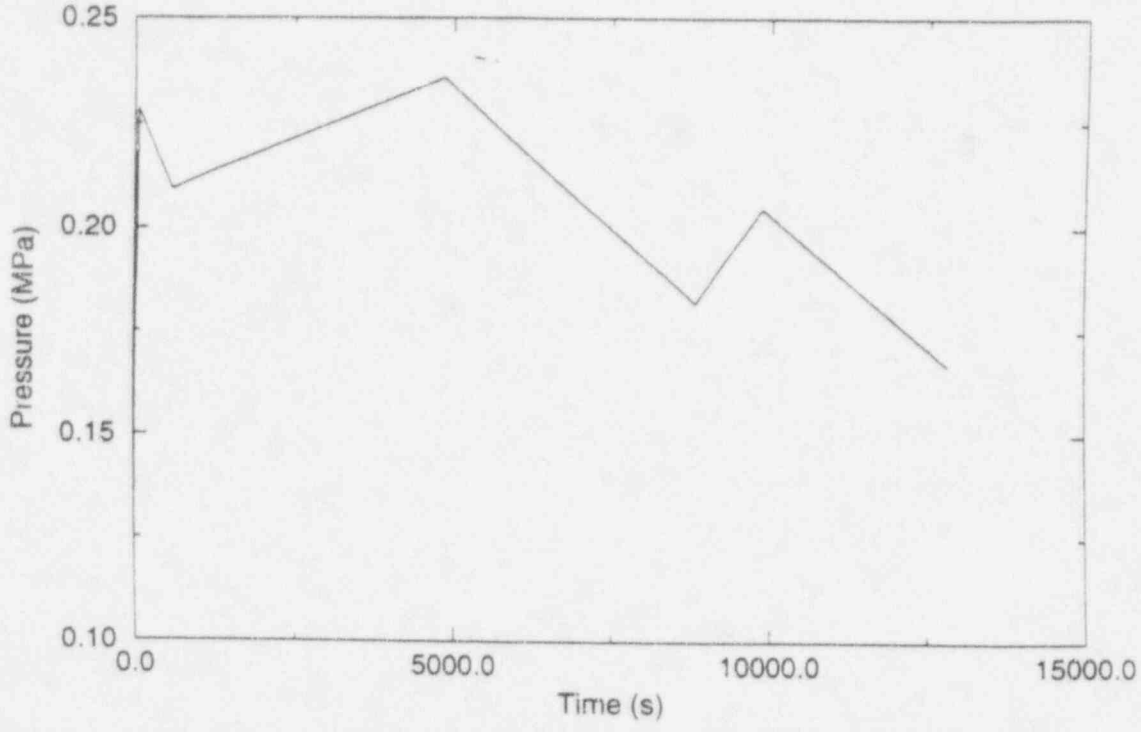

Figure 13. MAAP containment pressure[8] used as a SCDAP/RELAP5 boundary condition.

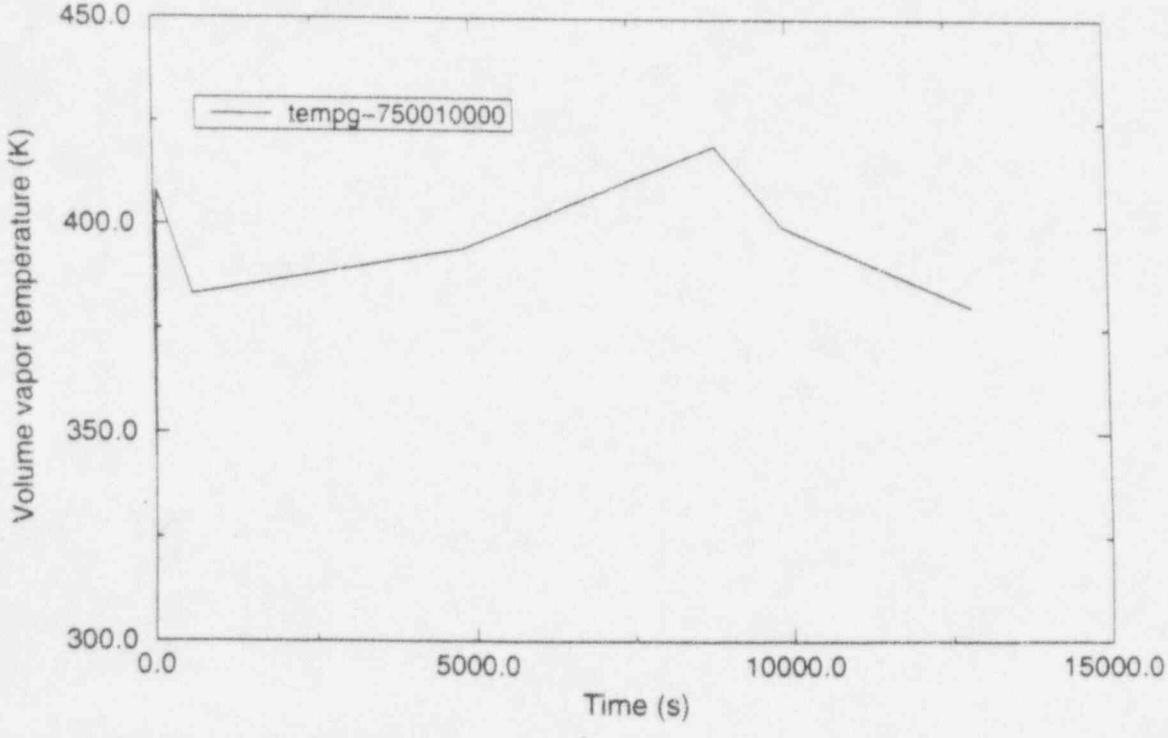

Figure 14. MAAP containment vapor temperature[8] used as a SCDAP/RELAP5 boundary condition.

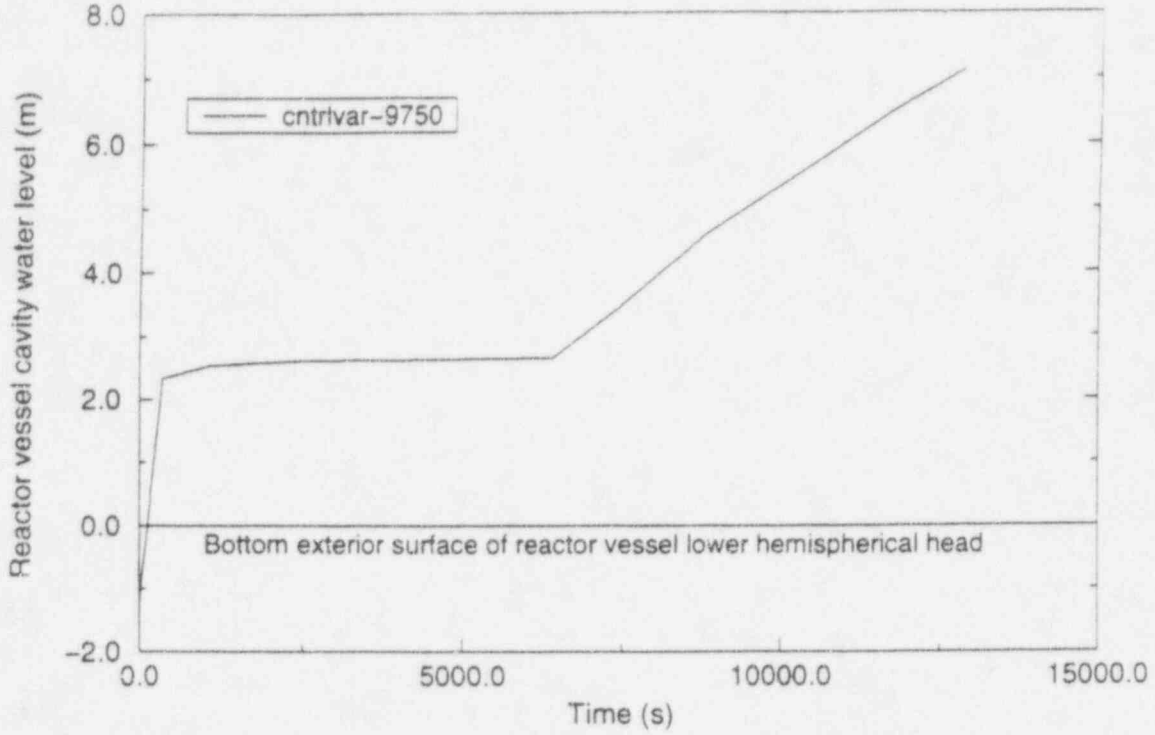

Figure 15. MAAP containment water level[8] used as a SCDAP/RELAP5 boundary condition.

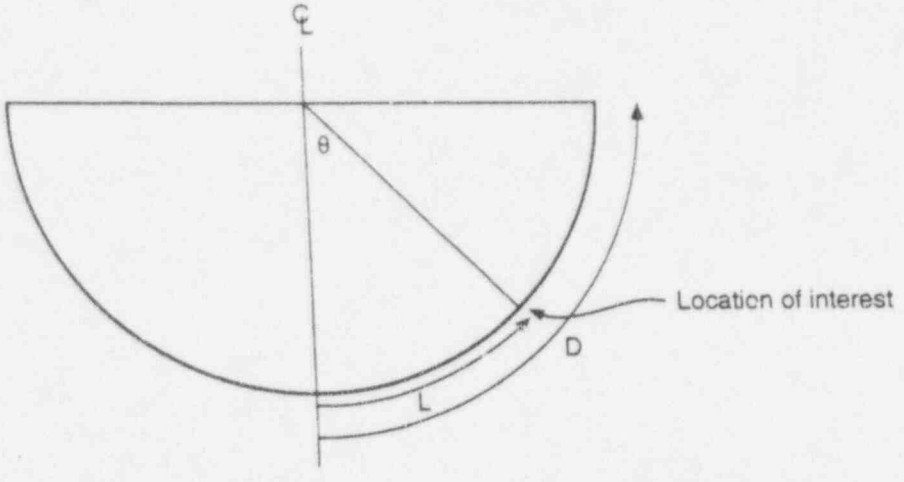

Figure 16. Orientation for calculation of boiling heat transfer from a hemispherical surface.

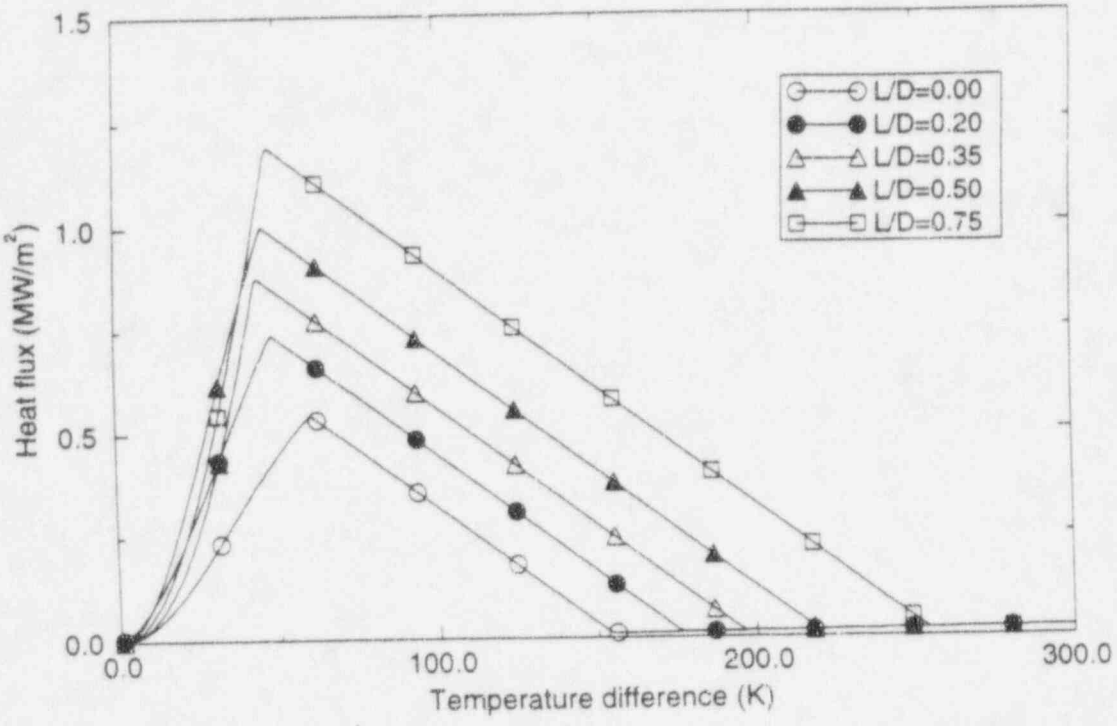

Figure 17. Predicted heat flux to a subcooled pool from lower head heat transfer correlations as a function of position and temperature difference.[6,7]

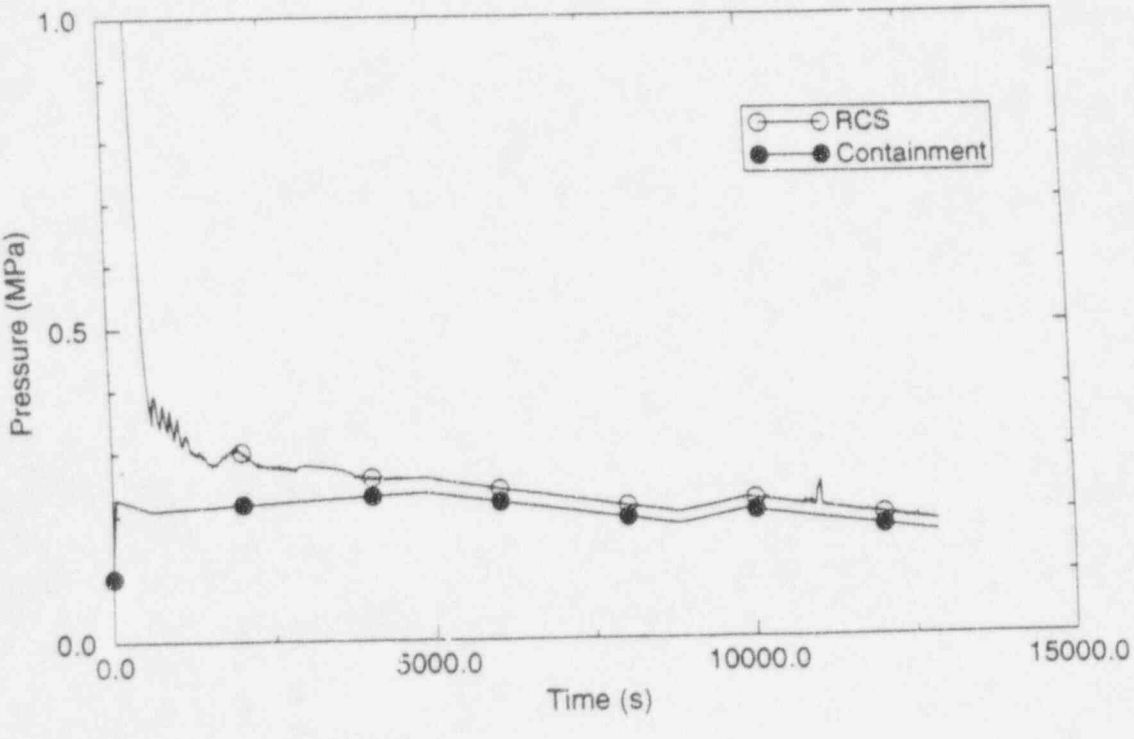

Figure 18. RCS and containment pressures.

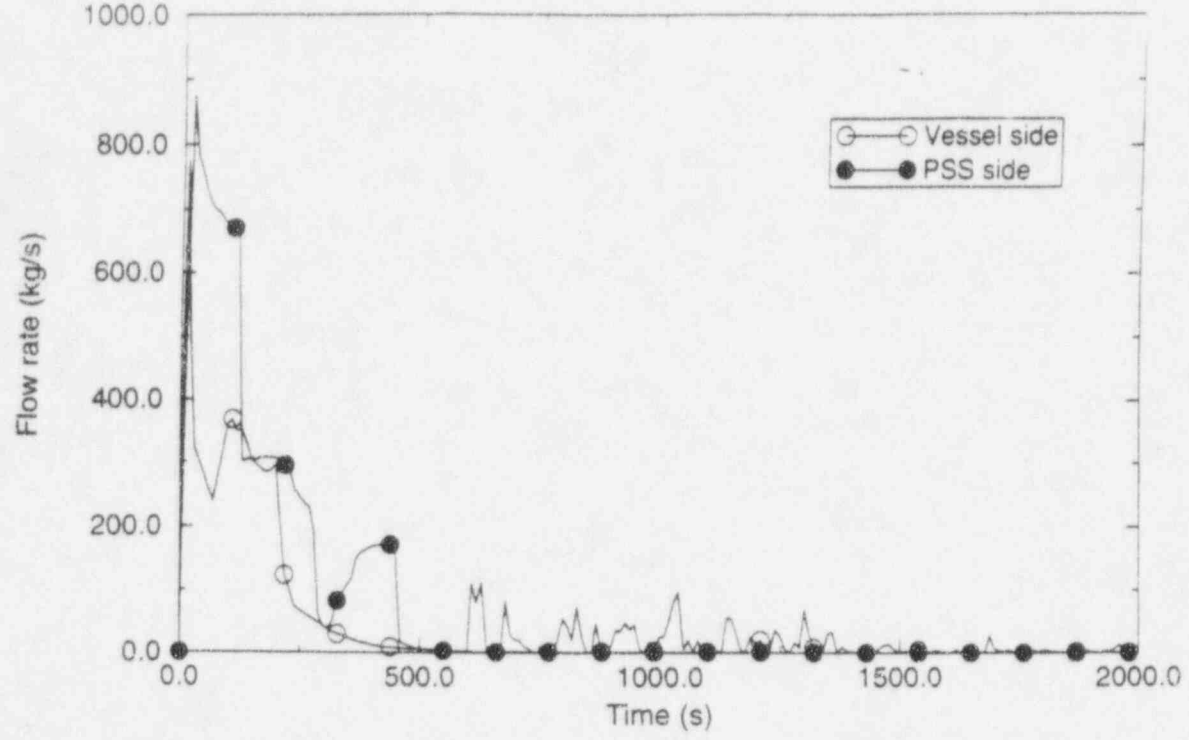

Figure 19. DVI2 break flows.

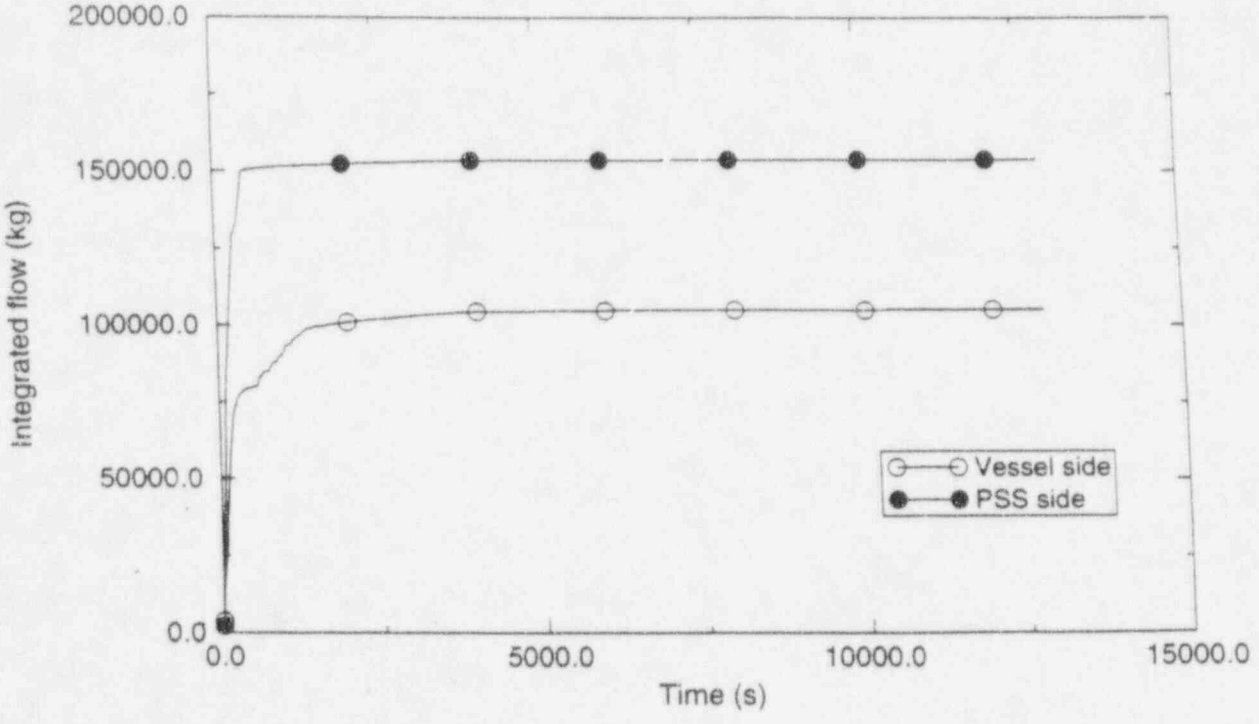

Figure 20. DVI2 integrated break flows.

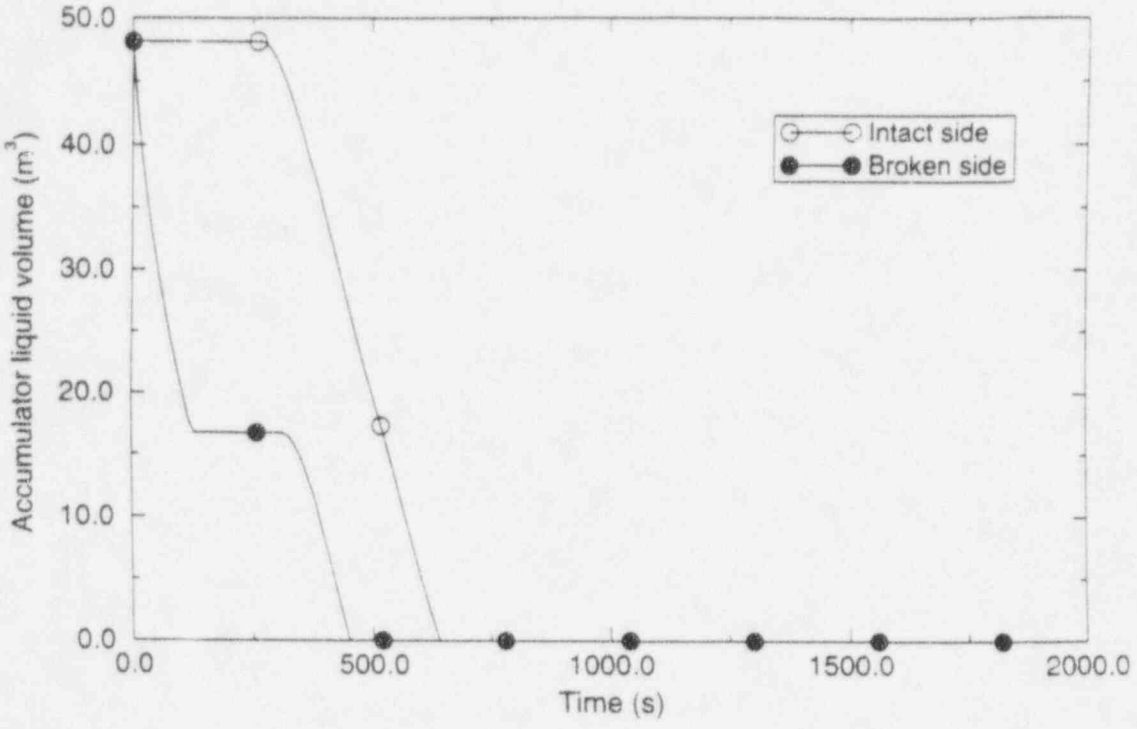

Figure 21. Accumulator liquid volumes.

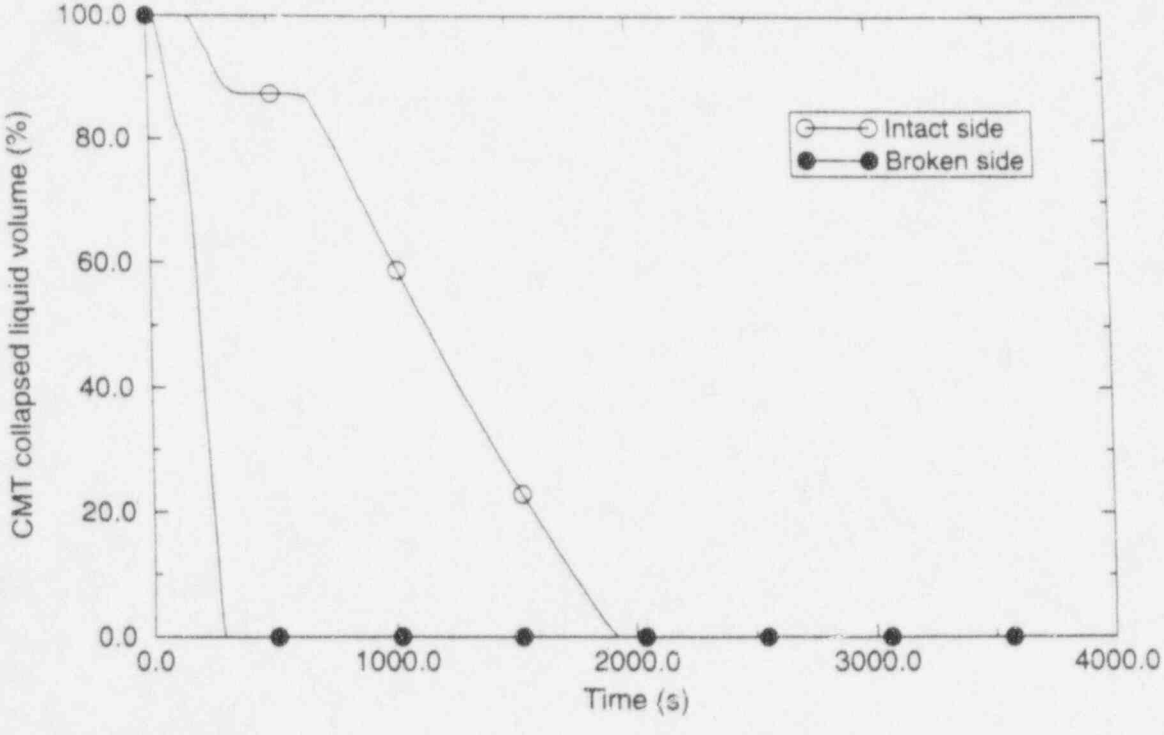

Figure 22. CMT liquid volumes.

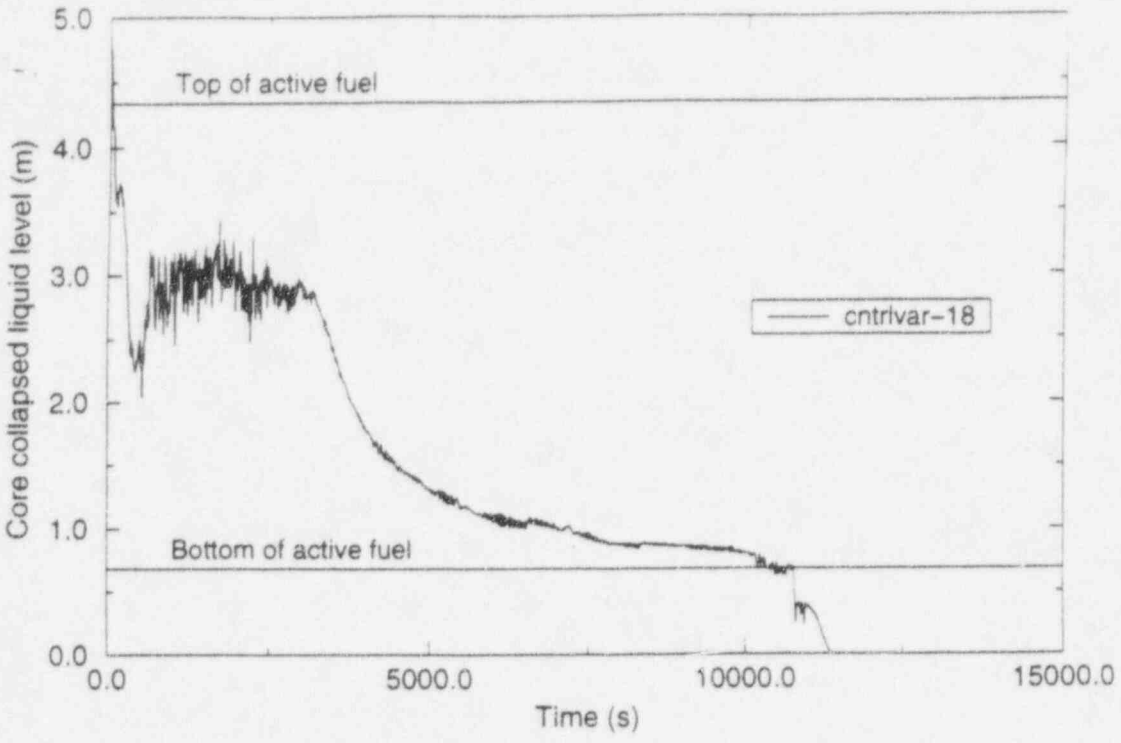

Figure 23. Core collapsed liquid level relative to the bottom of the lower core plate.

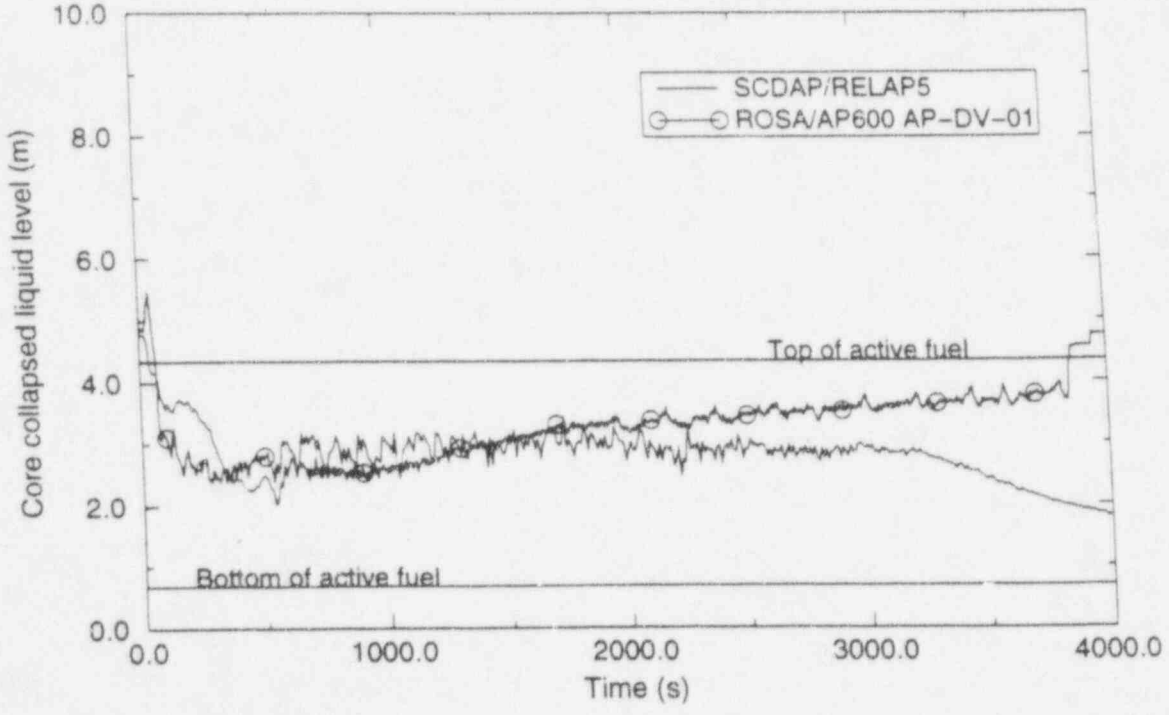

Figure 24. Calculated core collapsed liquid level compared to ROSA/AP600 experimental data[14] relative to the bottom of the lower core plate.

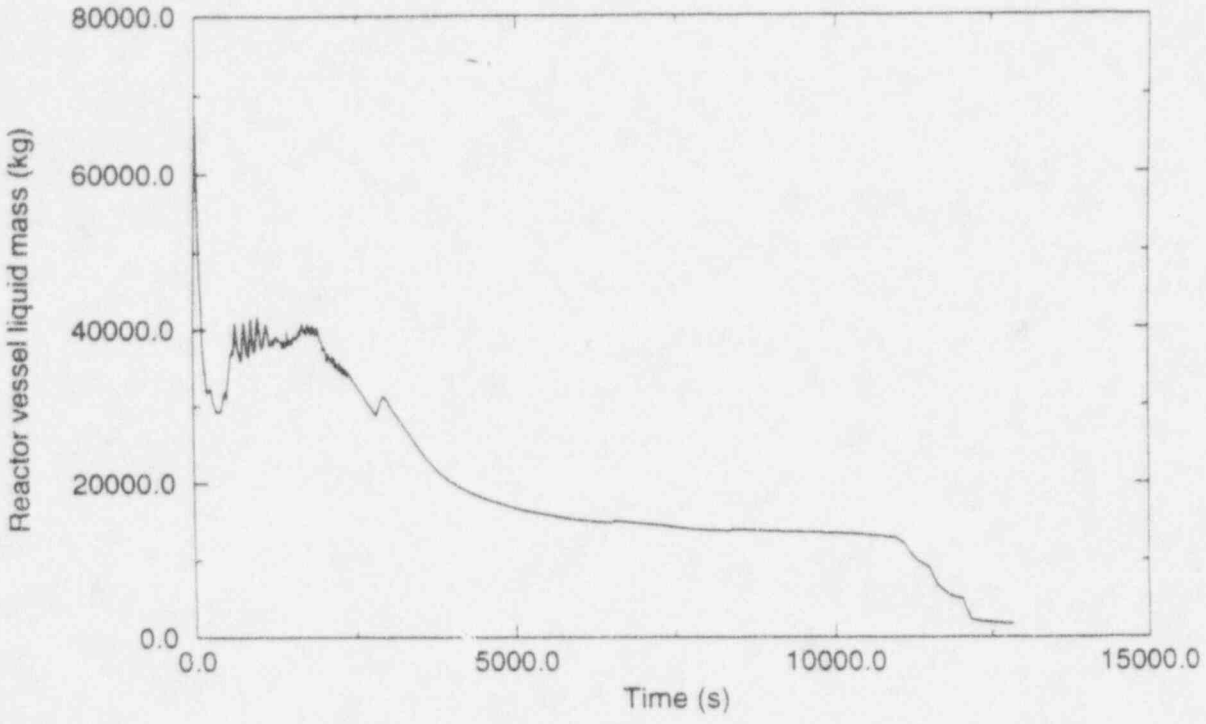

Figure 25. Reactor vessel liquid mass.

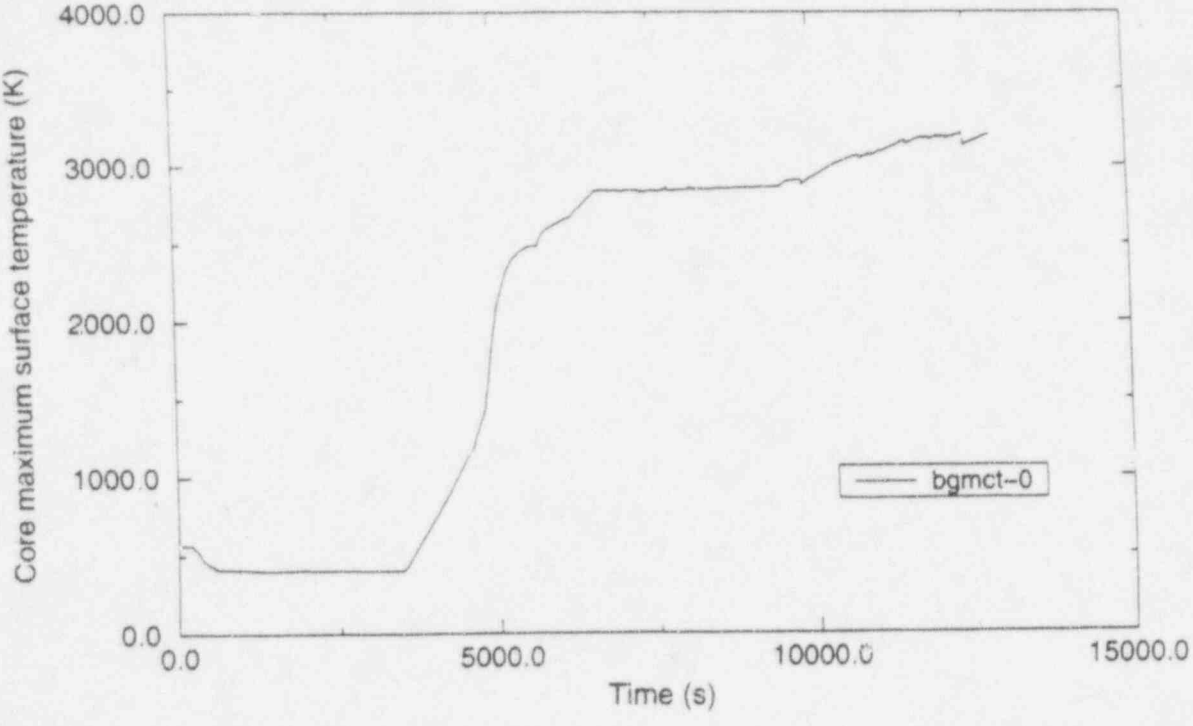

Figure 26. Maximum core surface temperature.

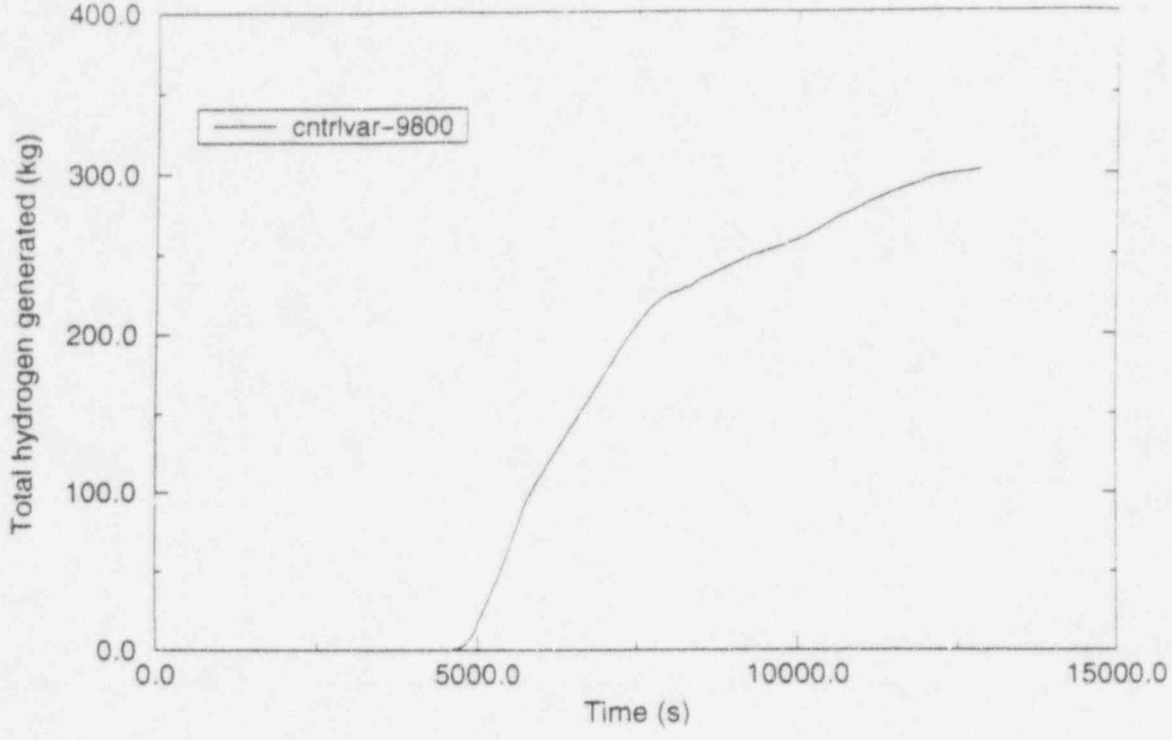

Figure 27. Total hydrogen generated.

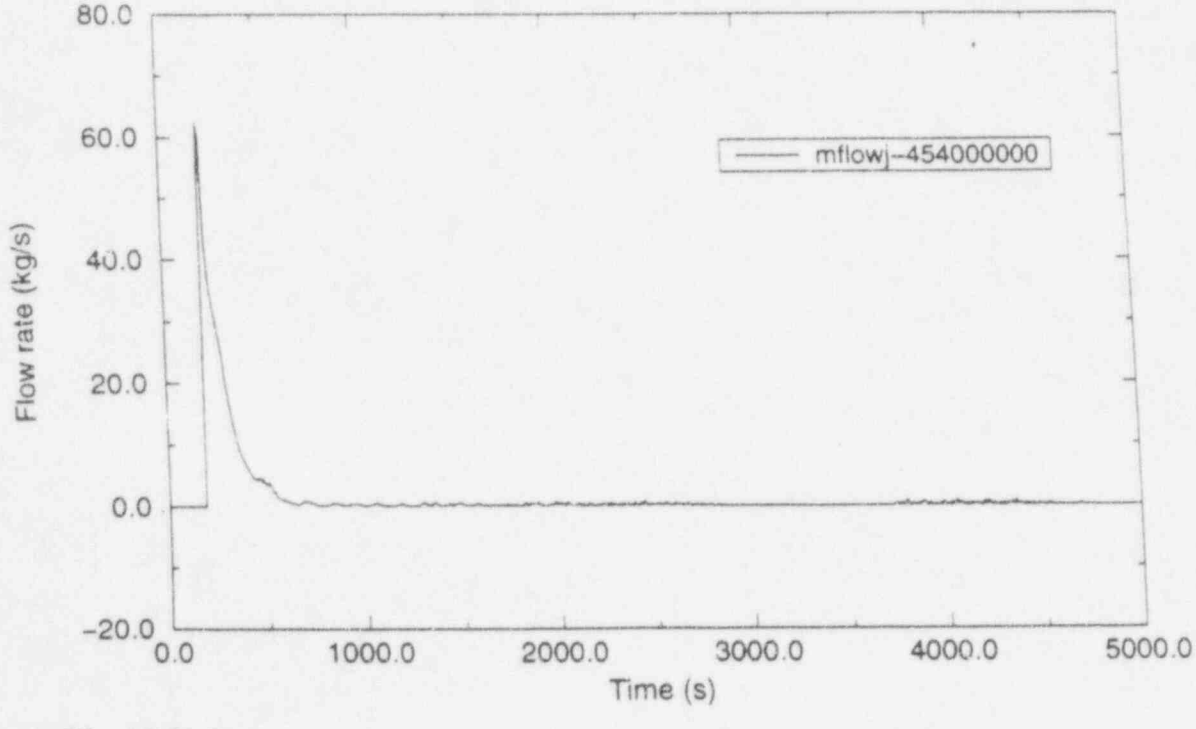

Figure 28. ADS1 flow.

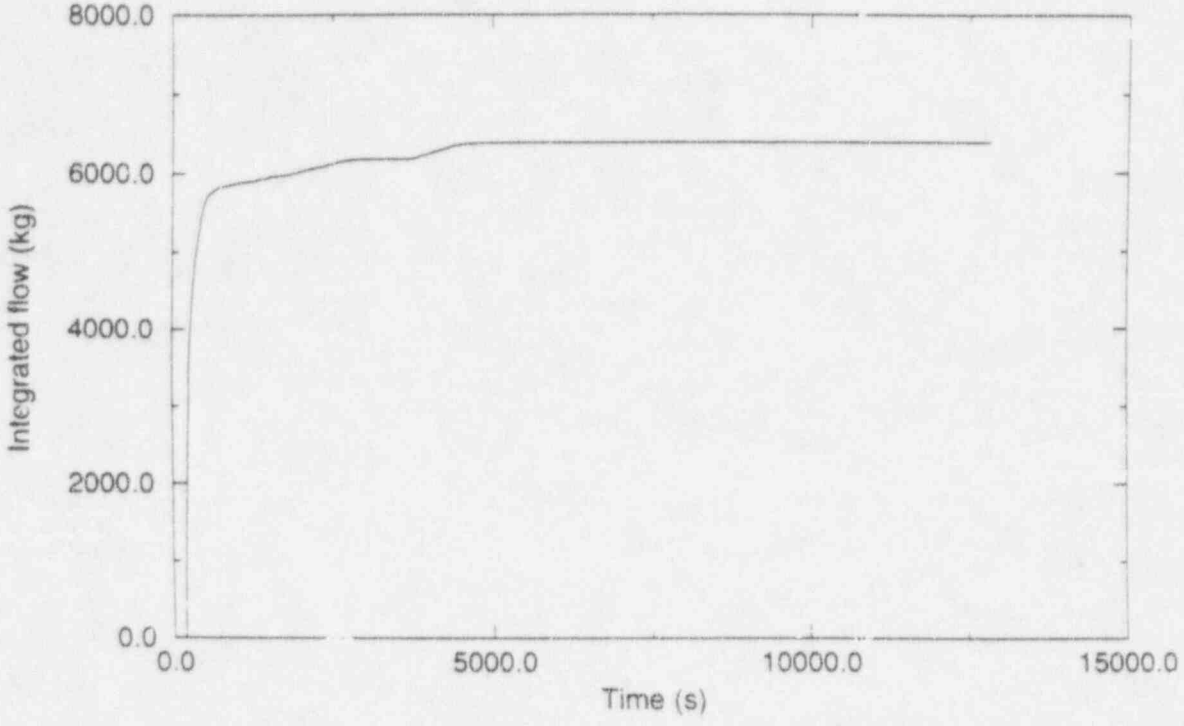

Figure 29. ADS1 integrated flow.

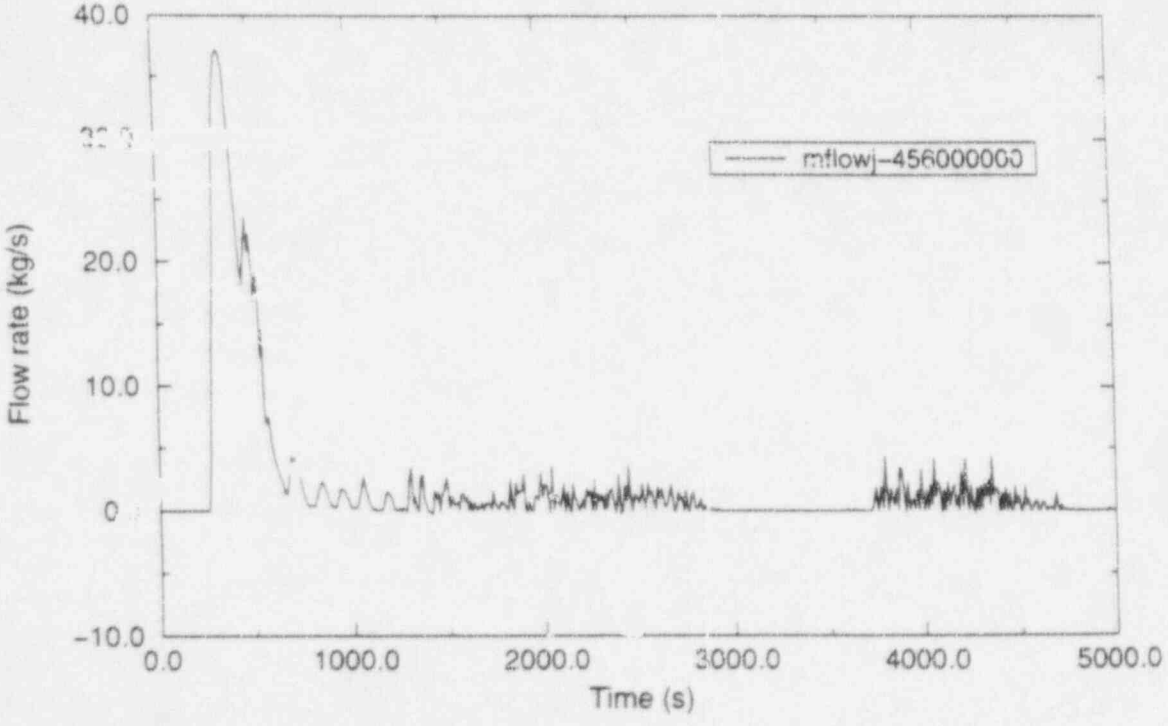

Figure 30. ADS2 flow.

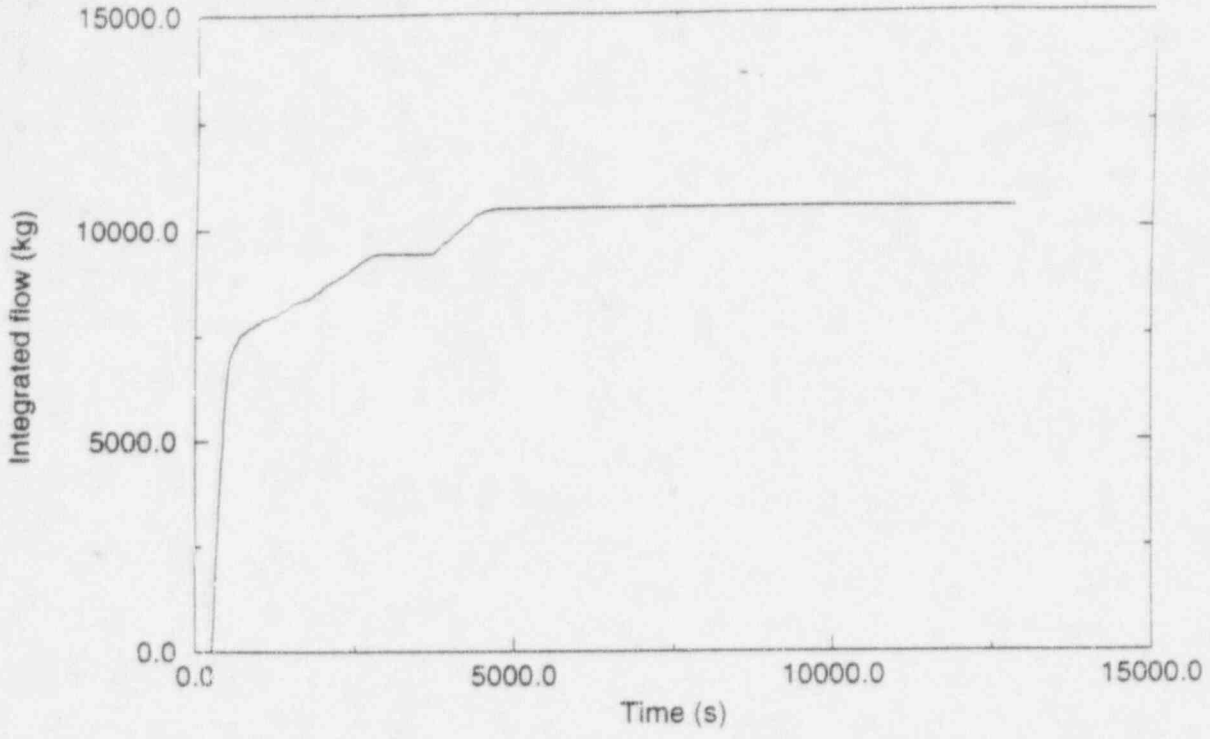

Figure 31. ADS2 integrated flow.

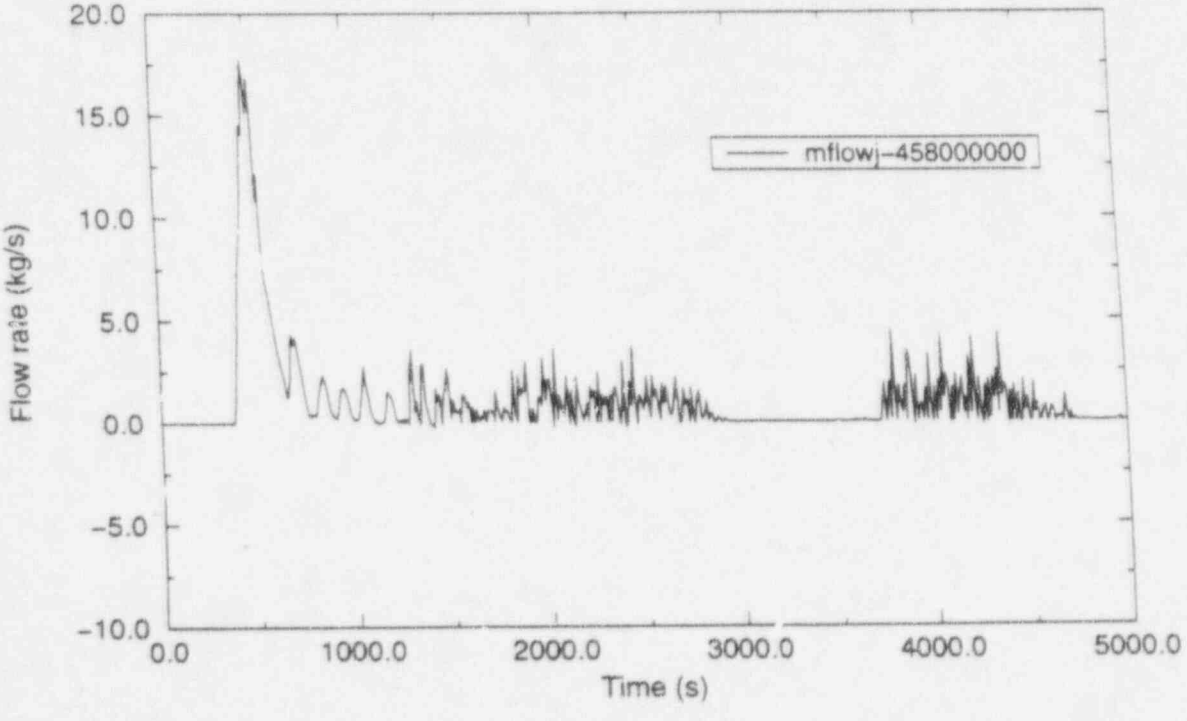

Figure 32. ADS3 flow.

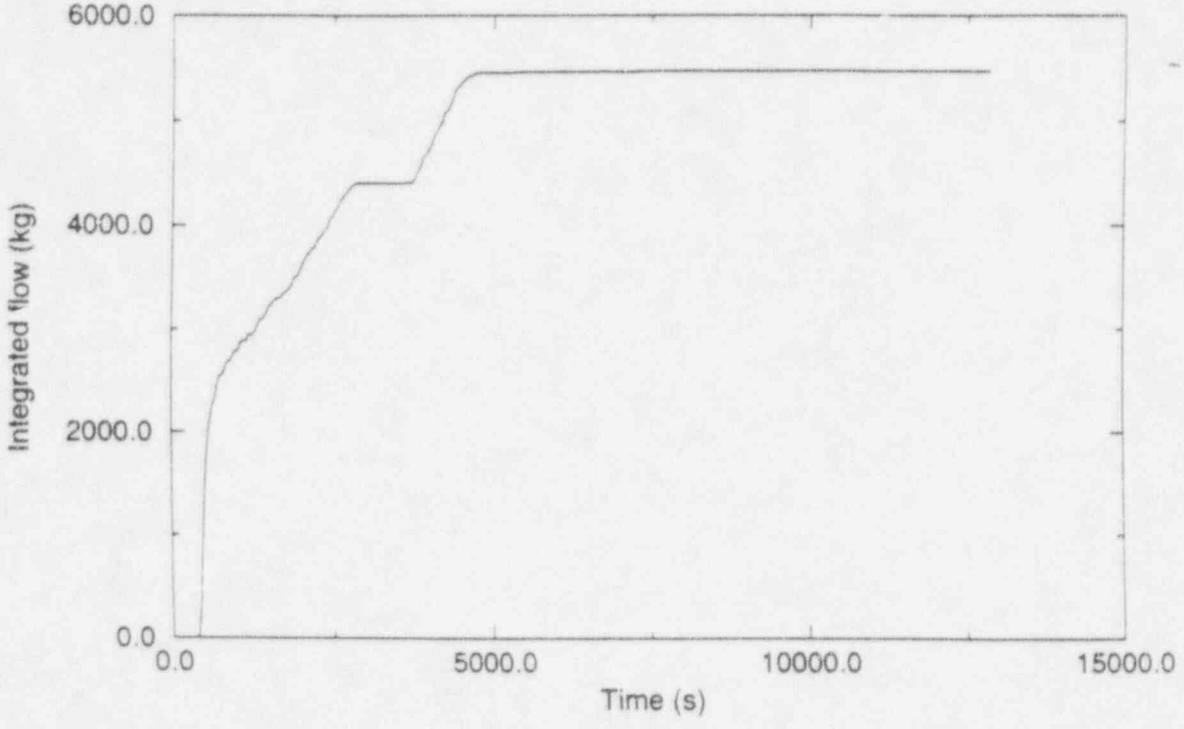

Figure 33. ADS3 integrated flow.

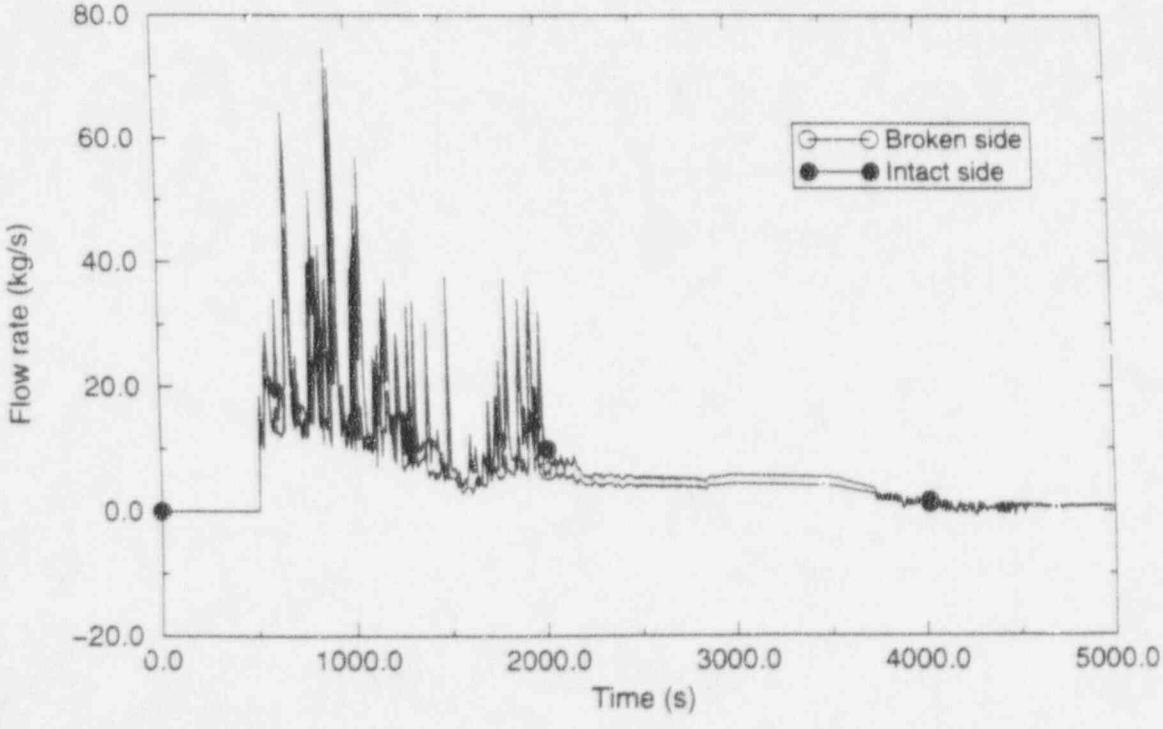

Figure 34. ADS4 flows.

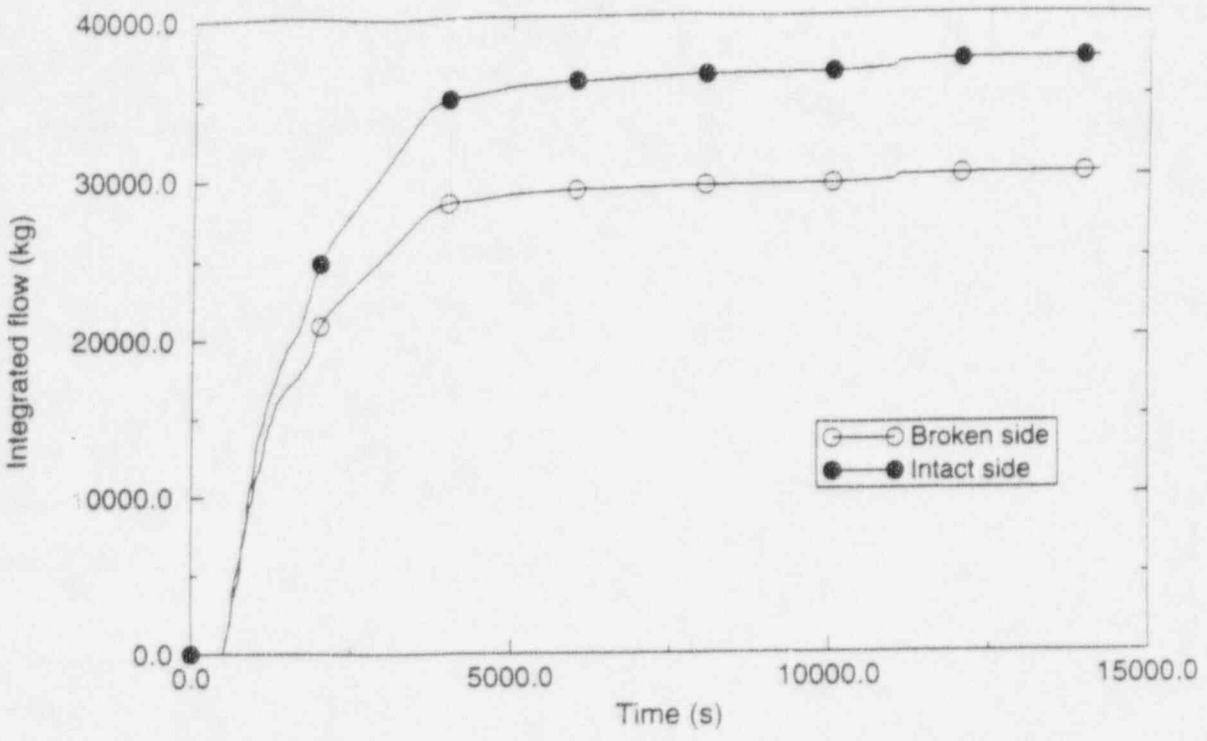

Figure 35. ADS4 integrated flows.

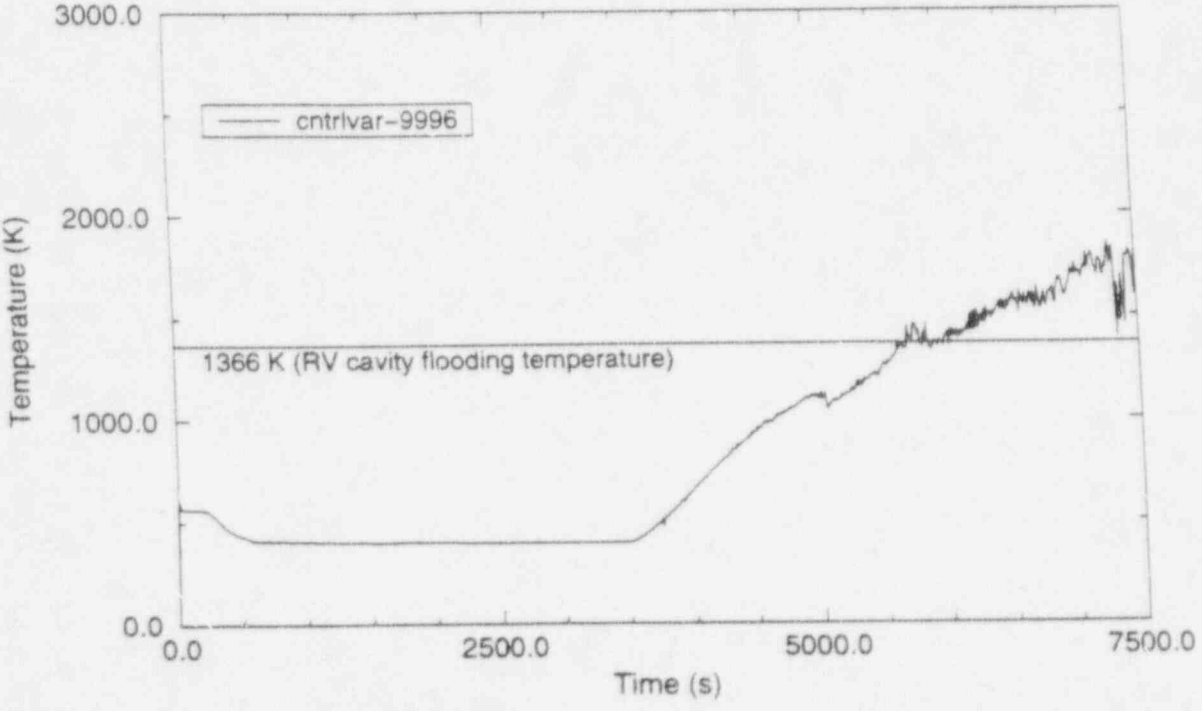

Figure 36. Average core outlet vapor temperature.

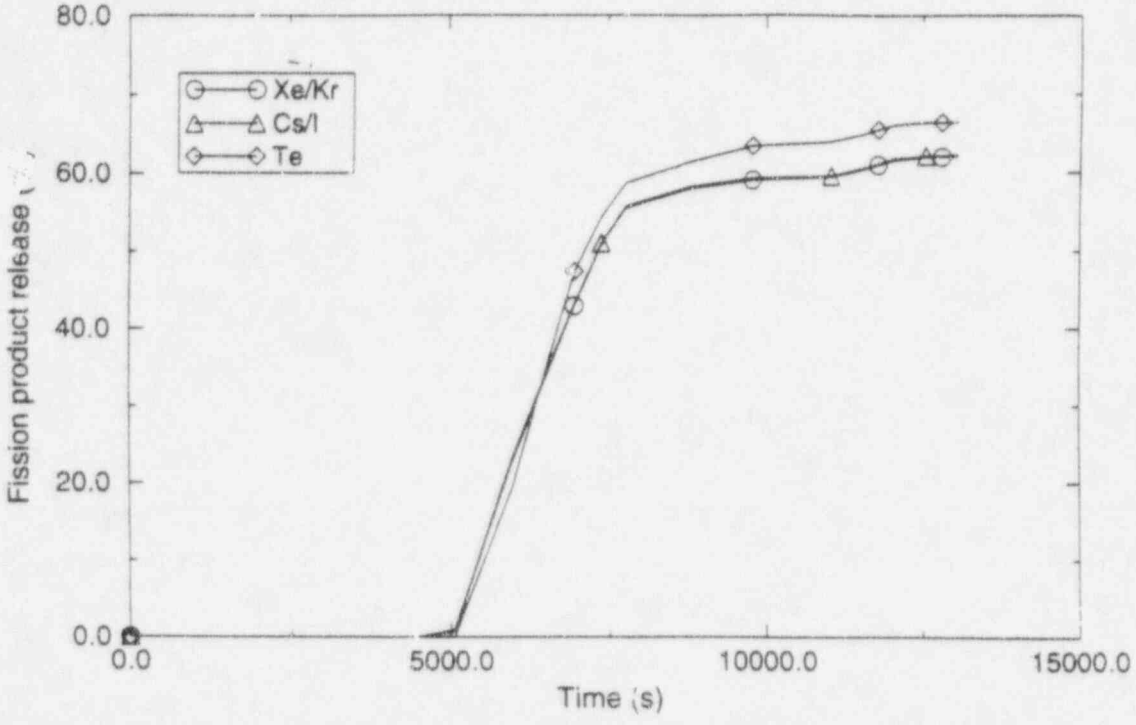

Figure 37. Fraction of fission products released from the fuel.

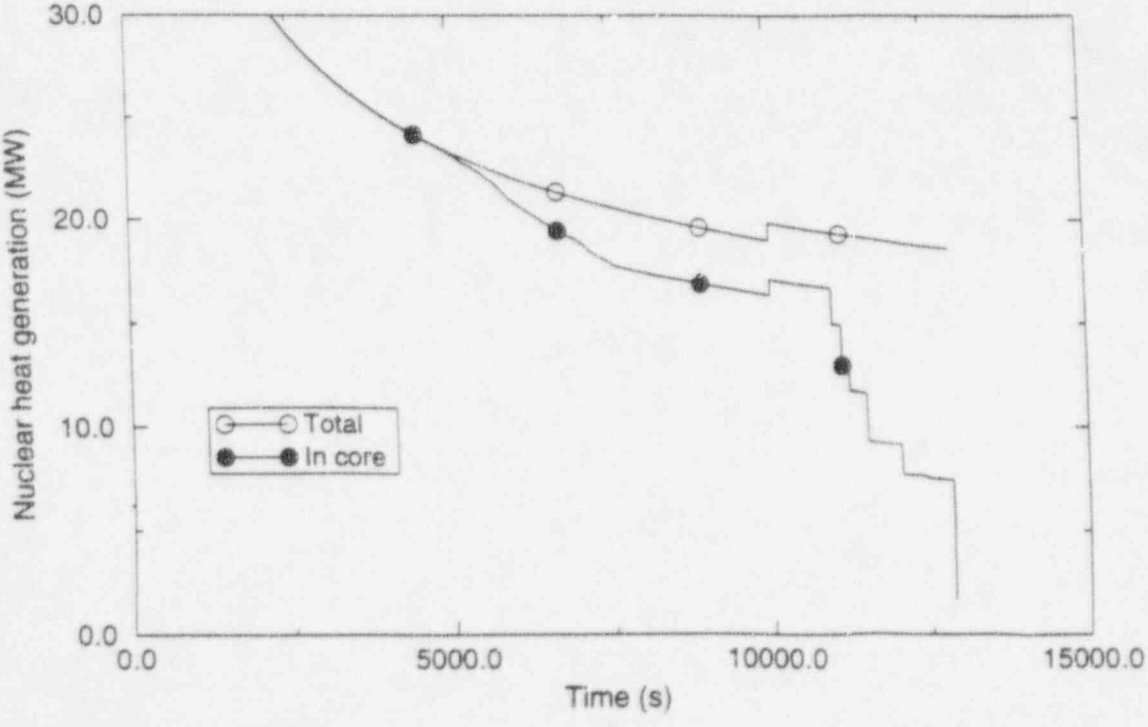

Figure 38. Decay power distribution.

Table 1. SCDAP components used to represent the AP600 core.

Component	Radial Division/Flow Channel	Description
1	1 / 113	Fuel rods
2	1 / 113	Control rods, instrument thimbles, empty guide thimbles
3	1 / 113	Gray rods
4	2 / 114	Fuel rods
5	2 / 114	Control rods, instrument thimbles, empty guide thimbles
6	2 / 114	Gray rods
7	3 / 115	Fuel rods
8	3 / 115	Control rods, instrument thimbles, empty guide thimbles
9	4 / 116	Fuel rods
10	4 / 116	Control rods, instrument thimbles, empty guide thimbles
11	4 / 116	Gray rods
12	5 / 117	Fuel rods
13	5 / 117	Instrument thimbles, empty guide thimbles
14	5 / 117	Stainless steel reflector, flat sections
15	5 / 117	Stainless steel reflector, corner sections

Table 2. Material masses in the active core region represented by SCDAP components.

Material	Mass (kg)
UO_2 (fuel) load	75 376
Stainless steel (reflectors, gray rods, and cladding; the reflector mass of ~6487 kg lying above and below the active core region was included in separate RELAP5 heat structures)	46 562
Zr (cladding, guide tubes, and spacers)	16 562
Ag-In-Cd (control rod absorber)	2771.1

Table 3. Coefficients used in a subcooled nucleate boiling correlation as a function of position on the exterior surface of the reactor vessel lower hemispherical head.[6]

Subcooled Boiling Correlation	Data Reported At	Correlation Applied At	Correlation Coefficients		
			a	b	c
1	L/D = 0	$0 < L/D \leq 0.1$	0	319	-2.83
2	L/D = 0.20	$0.1 < L/D \leq 0.275$	4016	430	-4.13
3	L/D = 0.35	$0.275 < L/D \leq 0.425$	0	337	2.61
4	L/D = 0.50	$0.425 < L/D \leq 0.625$	0	891	-9.04
5	L/D = 0.75	$L/D > 0.625$	0	529	0.08

Table 4. Subcooled boiling correlations and CHF for nodes on the exterior surface of the COUPLE mesh.

Surface Node Number	θ	L/D	Subcooled Boiling Correlation	CHF (MW/m^2)
1	0°	0	1	0.544
2	9.97°	0.111	2	0.655
3	19.0°	0.211	2	0.751
4	24.7°	0.275	2	0.811
5	30.6°	0.340	3	0.869
6	35.4°	0.394	3	0.915
7	40.4°	0.448	4	0.962
8	45.9°	0.510	4	1.01
9	51.1°	0.568	4	1.06
10	55.0°	0.612	4	1.09
11	59.1°	0.657	5	1.13
12	63.5°	0.705	5	1.16
13	68.1°	0.756	5	1.20
14	72.9°	0.810	5	1.24
15	77.9°	0.866	5	1.27
16	83.5°	0.928	5	1.31
17	> 90°	> 1	5	1.36
18	> 90°	> 1	5	1.36
19	> 90°	> 1	5	1.36
20	> 90°	> 1	5	1.36
21	> 90°	> 1	5	1.36
22	> 90°	> 1	5	1.36

Table 5. Sequence of transient events.

Event	Time (s)
Double-ended break in the DVI2 pipe (transient initiation)	0
Low-1 pressurizer pressure (< 13.20 MPa)	10.185
Low-1 pressurizer pressure signal (low-1 pressurizer pressure plus 0.7 s delay)	10.885
Reactor scrams on low-1 pressurizer pressure signal	10.885
Low-2 pressurizer pressure (< 12.86 MPa)	11.655
Low-2 pressurizer pressure signal (low-2 pressurizer pressure plus 1.2 s delay)	12.855
S-signal on low-2 pressurizer pressure signal	12.855
CMT actuation (both sides) on S-signal	12.855
RCPs trip and begin coastdown on CMT actuation plus 15 s delay	27.865
Core collapsed liquid level falls below the top of the active fuel	37.868
Reactor vessel cavity water level reaches the bottom of the lower hemispherical head	132.65
CMT2 level < 67.5%	176.21
ADS1 actuation signal (after CMT actuation and either CMT level < 67.5%)	176.22
ADS1 (1 train/1 valve) begins to open on actuation plus 20 s delay	196.23
ADS2 actuation signal (60 s after ADS1 actuation signal)	236.22
CMT2 level < 20%	246.80
ADS2 (1 train/1 valve) begins to open on actuation plus 30 s delay	266.22
CMT2 empties	325.76
ADS3 actuation signal (120 s after ADS2 actuation signal)	356.22
ADS3 (1 train/1 valve) begins to open on actuation plus 30 s delay	386.23
Accumulator-2 empties	460.00
ADS4-1 actuation signal (120 s after ADS3 actuation and either CMT level < 20%)	476.23
ADS4-2 actuation signal (30 s after ADS4-1 actuation)	506.23
ADS4-1 (1 train/1 valve) begins to open on actuation plus 30 s delay	506.23
ADS4-2 (1 train/1 valve) begins to open on actuation plus 30 s delay	536.23
Accumulator-1 empties	640.00
CMT1 level < 67.5%	908.60
CMT1 level < 20%	1573.9

Table 5. Sequence of transient events. (continued)

Event	Time (s)
CMT1 empties	1971.2
First fuel clad failure (Component 4, Fuel Level 12)	4455.0
Core outlet temperature reaches 1366 K	5666.3
First fuel (ceramic) melting occurs (Component 4, Fuel Level 8)	6594.9
Reactor vessel cavity water level reaches elevation of the bottom of the lower core plate	6777.0
Core collapsed liquid level falls below the bottom of the active fuel	10 346
First fuel melting adjacent to the reflector (Fuel Level 7)	10 782
First reflector failure (melt through, Component 14, Fuel Level 7)	10 970
First relocation into the lower head (via reflector failure, Component 14, Fuel Level 7)	10 970
Reflector failure (melt through, Component 14, Fuel Level 6)	11 126
Relocation into the lower head (via reflector failure, Component 14, Fuel Level 6)	11 126
Relocation into the lower head (thru failed reflector, Component 14, Fuel Level 6)	11 232
Reflector failure (melt through, Component 14, Fuel Level 5)	11 513
Relocation into the lower head (via reflector failure, Component 14, Fuel Level 5)	11 513
First relocation of control rod materials (Ag-In-Cd) into the lower head	11 891
Relocation of control rod materials into the lower head	11 987
Reflector failure (melt through, Component 14, Fuel Level 4)	12 047
Relocation into the lower head (via reflector failure, Component 14, Fuel Level 4)	12 047
Relocation of control rod materials into the lower head	12 189
Relocation of control rod materials into the lower head	12 263
Relocation of control rod materials into the lower head	12 431
First molten penetration through the bottom of the active fuel (Component 4)	12 844
First relocation into the lower head through the lower core plate	12 844
End of calculation with lower head debris including -63 995 kg of UO_2, -7586.4 kg of ZrO_2, -5572.6 kg of Zr, -2771.1 kg of Ag-In-Cd, and -3350.9 kg of stainless steel	12 844

Table 6. Summary of relocation events.

Time (s)	Relocated Mass (kg)					Temperature of Relocated Material (K)	Relocated Material Decay Power (MW)
	UO_2	ZrO_2	Zr	S. Steel	Ag-In-Cd		
10 970	7 145.4	806.72	822.48	556.24[a]		3076	1.730
11 126	8 428.0	964.24	863.46	1341.7[b]		3095	2.116
11 232	4 559.3	524.77	463.93	157.25[c]		3115	0.982
11 513	10 478	1226.1	1046.3	342.76[d]		3145	2.295
11 891					956.41	1073	
11 987					627.79	1073	
12 047	6 596.3	792.43	638.07	205.13[e]		3182	1.416
12 189					954.20	1073	
12 263					174.20	1073	
12 431					58.500	1073	
12 844	26 788	3277.6	1732.9	747.82[f]		3199	5.779
	63 995	7591.9	5567.1	3350.9	2771.1	Relocated Mass Totals	

a. Includes 453.06 kg of lower plenum structural stainless steel at a temperature of 393 K that was submerged during relocation.
b. Includes 1220.0 kg of lower plenum structural stainless steel at a temperature of 416 K that was submerged during relocation.
c. Includes 91.410 kg of lower plenum structural stainless steel at a temperature of 438 K that was submerged during relocation.
d. Includes 191.45 kg of lower plenum structural stainless steel at a temperature of 427 K that was submerged during relocation.
e. Includes 109.88 kg of lower plenum structural stainless steel at a temperature of 417 K that was submerged during relocation.
f. Includes 361.00 kg of lower plenum structural stainless steel at a temperature of 410 K that was submerged during relocation.